doi : 10.17596/0003800

JAMSTEC *Chikyu* SCORE Expedition 913

Preliminary Cruise Report

Reconstruction of the Kuroshio state for super interglacials during the Brunhes chron

Minoru Ikehara (Kochi Univ.), Yuki Morono (JAMSTEC), Takuya Sagawa (Kanazawa Univ.), Natsumi Okutsu (JAMSTEC) and the Exp.913 Shipboard Scientists

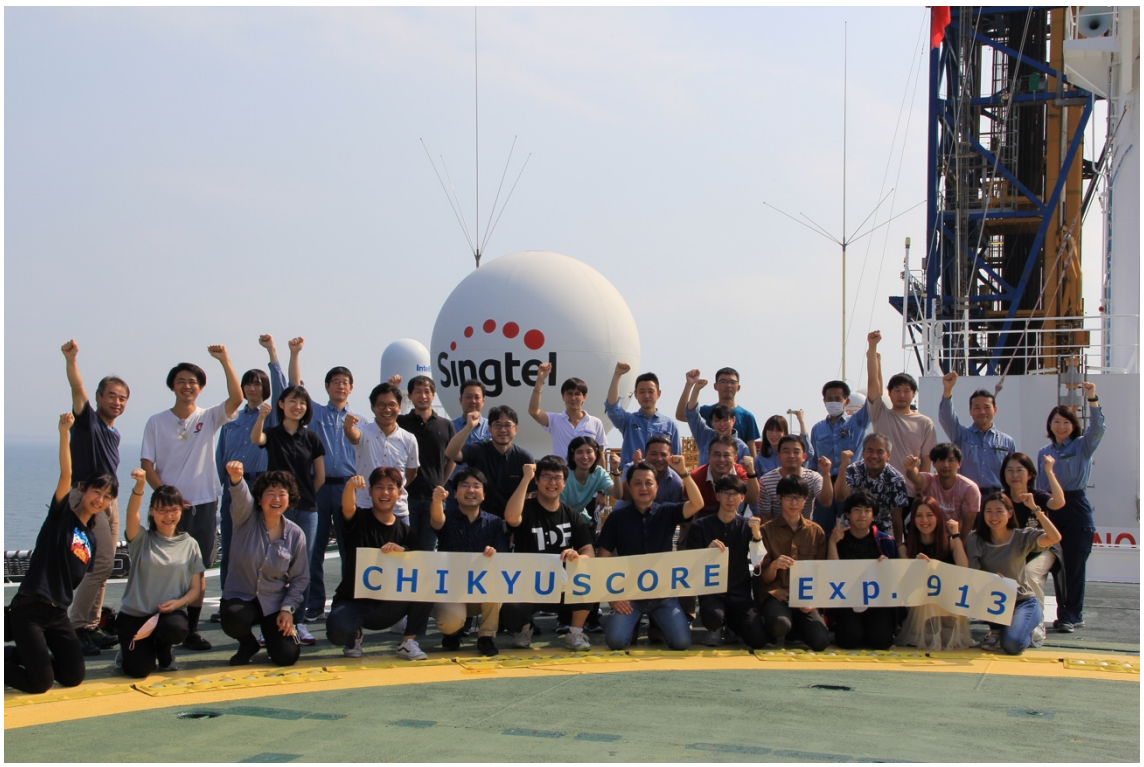

Acknowledgements

Expedition 913 shipboard scientists thank all the MQJ drilling staff and MWJ laboratory technical staff of the D/V Chikyu for the wonderful cruise and taking high-quality core samples. Special thanks MarE3 Operation Superintendent of the expedition for successful sampling. The proponents would like to thank J-DESC and MarE3 for providing the opportunity of this short expedition.

Contents

1. Cruise Information

Cruise ID: CK21-S01, Exp. 913
Name of vessel: D/V Chikyu
Proposal representative: Minoru Ikehara (Kochi University)
Cruise period: August 22nd, 2021 - August 31st, 2021
Ports of departure / arrival: Shimizu / Shimizu

2. Expedition 913 Shipboard scientists

Minoru Ikehara (Chief scientist, Lead Proponent, Paleoceanography)
Center for Advanced Marine Core Research, Kochi University
Yuki Morono (Associate-chief scientist, Microbiology)
Kochi Institute for Core Sample Research, JAMSTEC
Takuya Sagawa (Geochemistry)
Institute of Science and Engineering, Kanazawa University
Goichiro Uramoto (Sedimentology)
Center for Advanced Marine Core Research, Kochi University
Takuya Matsuzaki (Technical staff)
Center for Advanced Marine Core Research, Kochi University
Yuki Fujimura ((Technical staff)
Center for Advanced Marine Core Research, Kochi University
Akira Ijiri (Geochemistry)
Graduate School of Maritime Sciences, Kobe University
Fumiaki Mori (Microbiology)
Kochi Institute for Core Sample Research, JAMSTEC
Ryo Yamaoka (Technical staff)
Kochi Institute for Core Sample Research, JAMSTEC
Fumito Shiraishi (sedimentology)
Graduate School of Advanced Science and Engineering, Hiroshima University
Kenji M. Matsuzaki (micropaleontology)
Atmosphere and Ocean Research Institute, The University of Tokyo
Ayumi Maeda (micropaleontology)
Geological Survey of Japan, AIST
Hana Ishii (organic geochemistry)
Graduate School of Environmental Science, Hokkaido University

Keita Kono (geochemistry)

Faculty of Science and Technology, Kochi University

Takuto Kasuya (micropaleontology)

Graduate School of Science, Kyushu University

Daisuke Kuwano (micropaleontology)

Graduate School of Science and Engineering, Chiba University

Mako Takada (microbiology)

Graduate School of Frontier Sciences, The University of Tokyo

Yuya Hashimoto (geochemistry)

Graduate School of Natural Science and Technology, Kanazawa University

Keisuke Furukawa (organic geochemistry)

Graduate School of Environmental Science, Hokkaido University

Masashi Ikeda (organic geochemistry)

Graduate School of Science, Hokkaido University

Natsumi Okutsu (Expedition Project Manager)

MarE3, JAMSTEC

3. Introduction

3.1 Nature of the Kuroshio Current during the past “super interglacials”

In the North Pacific, the Kuroshio Current (KC) is a strong western boundary current and supplies heat and water vapor from the tropical Pacific to the subarctic, influencing climate conditions over the East Asia including the Japanese Islands (Fig. 1). An atmosphere-ocean coupled climate model shows that the velocity of the KC would increase (Sakamoto et al., 2005) and the Kuroshio Extension (KE) will shift northward (Yang et al., 2020) in response to the future global warming. As well as the KC, other western boundary currents, such as Gulf stream in the Atlantic and Agulhas Current in the Indian Ocean are predicted to exhibit the increase in the volume transport under the future global warm conditions (Wu et al., 2012, Hu et al., 2015).

Marine Isotope Stage (MIS) 5e (~125 ka) and MIS 11c (~410 ka) are so-called the “super interglacials” since these periods were marked by warmer climate conditions than pre-industrial (Melles et al., 2012). The analyses of paleoclimate/paleoceanographic conditions during these “super interglacials” are strongly required because these studies provide us the potential to investigate the long-term stability of warmer climates and understand the impact of warmer climates on ecological and geomorphic systems (Candy et al., 2014). The interest in MIS 11 reflects the fact that it is widely suggested to be the most appropriate climate analogue for the Holocene (e.g., Droxler and Farrell, 2000, Tzedakis, 2010), because the pattern of incoming solar insolation that occurred during MIS 11 matches that of the Holocene (e.g., Berger and Loutre, 2002).

If this is the case, the regional climate conditions over the Japanese Islands would be significantly influenced by the changes in the velocity of the KC. Furthermore, the past “super interglacials” are thought to be important analogues for the future global warming climate. However, at this moment, there are no reliable information on the volume transport and temperature of the KC during the past “super interglacials” due to a lack of the suitable sediment cores from the Northwest Pacific.

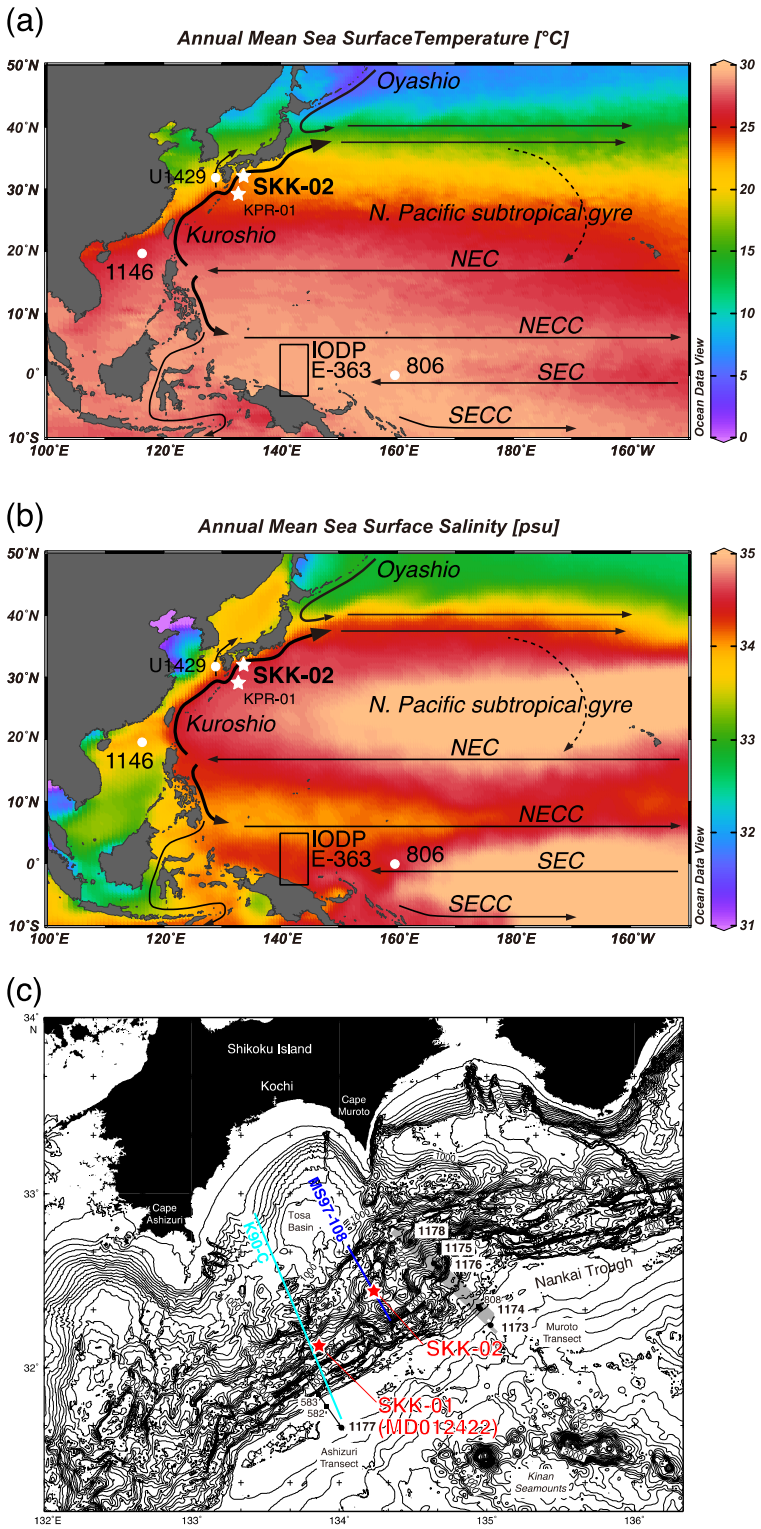

Figure 1. Map showing the Kuroshio Current and the North Pacific subtropical gyre with distributions of (a) sea surface temperature (Locarnini et al., 2013) and (b) salinity (Zweng et al., 2013) based on Would Ocean Atlas Data 2013 (WOA13). Proposed sites SKK-02 and SKK-01

and drilled sites in ODP/IODP are indicated on a map of annual averaged SST and SSS in the Pacific. (c) Locations of the primary site SKK-02 and alternate site SKK-01 on the topographic map from Moore et al., (2001). ODP Leg 190 (solid circles) and DSDP drill sites (solid squares) in the Nankai Trough are shown in the map. Seismic lines MS97-108 (blue line) and K90-C (light blue line) is also shown in the map.

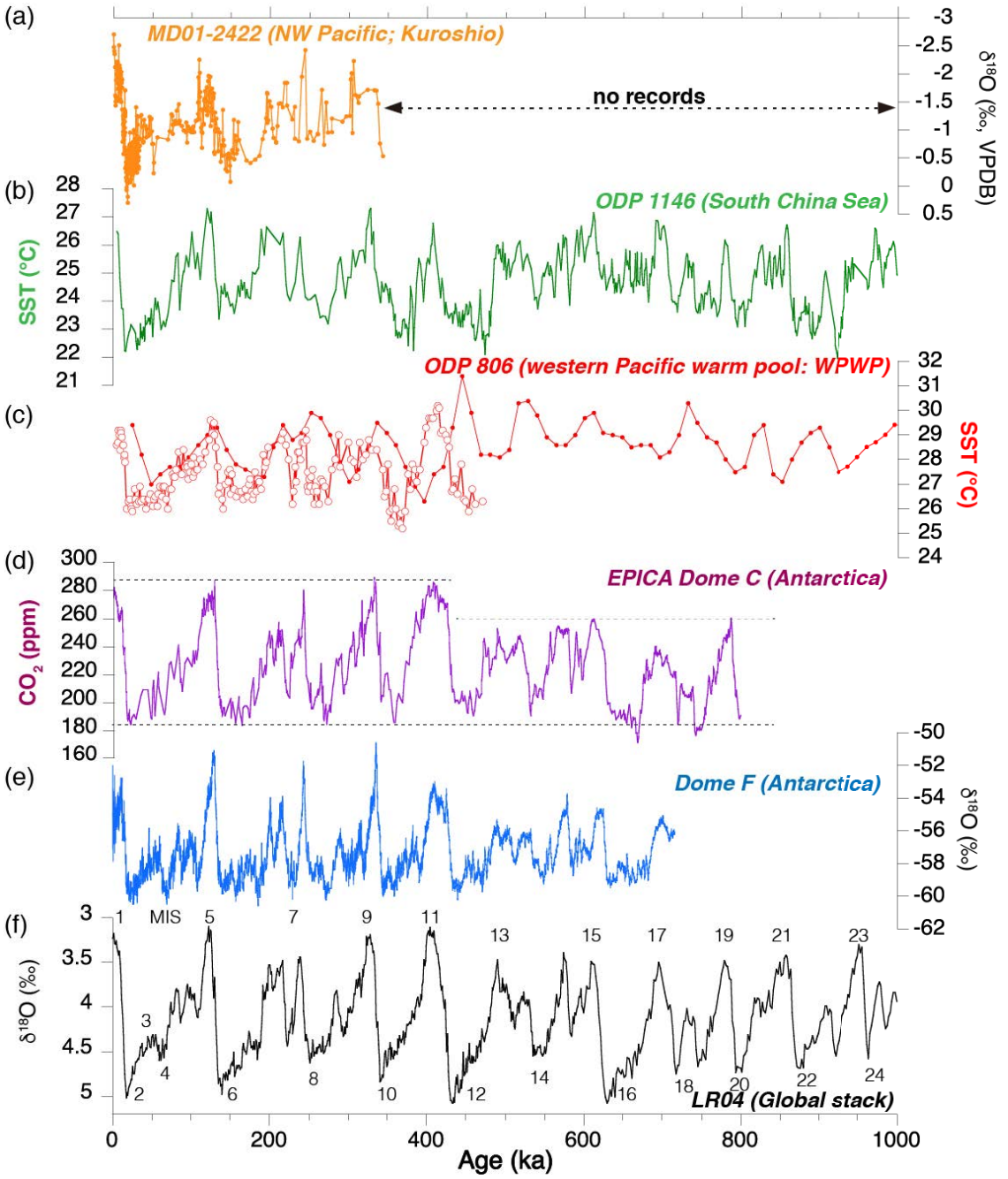

Figure 2. Proxy records over the past 1 Ma. (a) $\delta^{18}O$ changes in planktic foraminifer *Globigerinoides ruber* at the proposed site SKK-01 (core MD01-2422) off Shikoku in the

Northwest Pacific (low resolution data: Ikehara et al., 2006, high-resolution data: M. Ikehara. unpublished). (b) Uk37-based SST records from ODP Site 1146 in the South China Sea (Herbert et al., 2010). (c) Mg/Ca-based SST records from ODP Site 806 in the western Pacific warm pool (WPWP) (open circles: Lea et al., 2000; solid circles: Medina-Elizalde et al., 2008). (d) Variations of atmospheric CO_2 concentration in the Antarctic ice core EPICA Dome C (Luthi et al., 2008). (e) $\delta^{18}O$ records at the Antarctic ice core Dome Fuji (Uemura et al., 2018). (f) Global stacked benthic $\delta^{18}O$ records with Marine Isotope Stage (MIS) (Lisiecki and Raymo, 2005). The odd numbers show the interglacials, and the even numbers show the glacial stages.

4. Scientific objectives

State of knowledge and specific objectives

MIS 5e and MIS 11 are the warmer interglacial periods than pre-industrial, and many studies have been conducted based on marine and lake sediment cores. These studies show that the global mean annual surface temperature was ~1°C to 2°C warmer than pre-industrial and at least 2°C warmer at high latitudes (Turney and Jones, 2010; Otto-Bliesner et al., 2013). Greenland also experienced warming of 8°C ± 4°C at 126 ka than pre-industrial (NEEM community members, 2013). Further, for the MIS 11, although the number of studies are less than MIS 5e, Antarctic ice core and tropical Pacific paleo temperature estimates suggest that global temperature was 1.5°C to 2.0°C warmer than pre-industrial (Masson-Delmotte et al., 2013).

In the western North Pacific, long-term SST changes were investigated by using DSDP/ODP sediment cores (Wang., 1994, Etourneau et al., 2010, Lea et al., 2000, Medina-Elizalde et al., 2008, Jia et al., 2008, Herbert et al., 2010). Although Pliocene-Pleistocene SST records were reported based on the planktic foraminifera at DSDP sites in the western Pacific (Wang, 1994), but the time resolution was not sufficient to evaluate the glacial-interglacial SST changes in the Brunhes chron. Uk37-based SST record at ODP Site 1146 in the South China Sea (Herbert et al., 2010) show the distinct glacial-interglacial variations, and SST in MIS 5e and 9 represent slightly warmer than the Holocene (Fig. 2). Mg/Ca based SST records from ODP Site 806 in the western Pacific warm pool (WPWP) (Lea et al., 2000, Medina-Elizalde et al., 2008) indicate that the amplitude of SST changes in the tropical Pacific was ca. 3°C for glacial-interglacial cycles. These sites are located far from the end of the KC, which are not the representative for KC itself and not ideal records for evaluating regional climate conditions over the Japanese Islands under the influence of the changes in the velocity of the KC.

In addition, the drilling target area off Shikoku is also most suitable to investigate the detailed tephrostratigraphy in the Northwest Pacific (Fig. 3). In core MD01-2422 (SKK-01), well-dated widespread tephra horizons, Kikai-Akahoya (K-Ah; 7.3 ka) and Aira-Tn (AT; 30 ka), Aira-

Iwato (A-Iw), Aira-Fukuyama (A-Fk), Ata-Toihama (Ata-Th) and Kakuto (Kkt) were identified (Ikehara et al., 2006) (Fig. 3b). Core site off Shikoku lies within the westerly wind belt, therefore many volcanoes/calderas are upwind of the site (e.g. Kikai, Aira and Aso calderas in Kyushu island) (Fig. 3d). Thus, the drilling target area off Shikoku is an excellent sedimentary archive with high-time resolution (Fig. 3a).

Given the presently obtained sedimentary data and knowledge, we propose to drill a penetration depth of 100-m long sediment cores off Shikoku Island in the Northwest Pacific to address the following scientific issue.

Main Objective: How does the Kuroshio respond to "super interglacials" compared to pre-industrial?

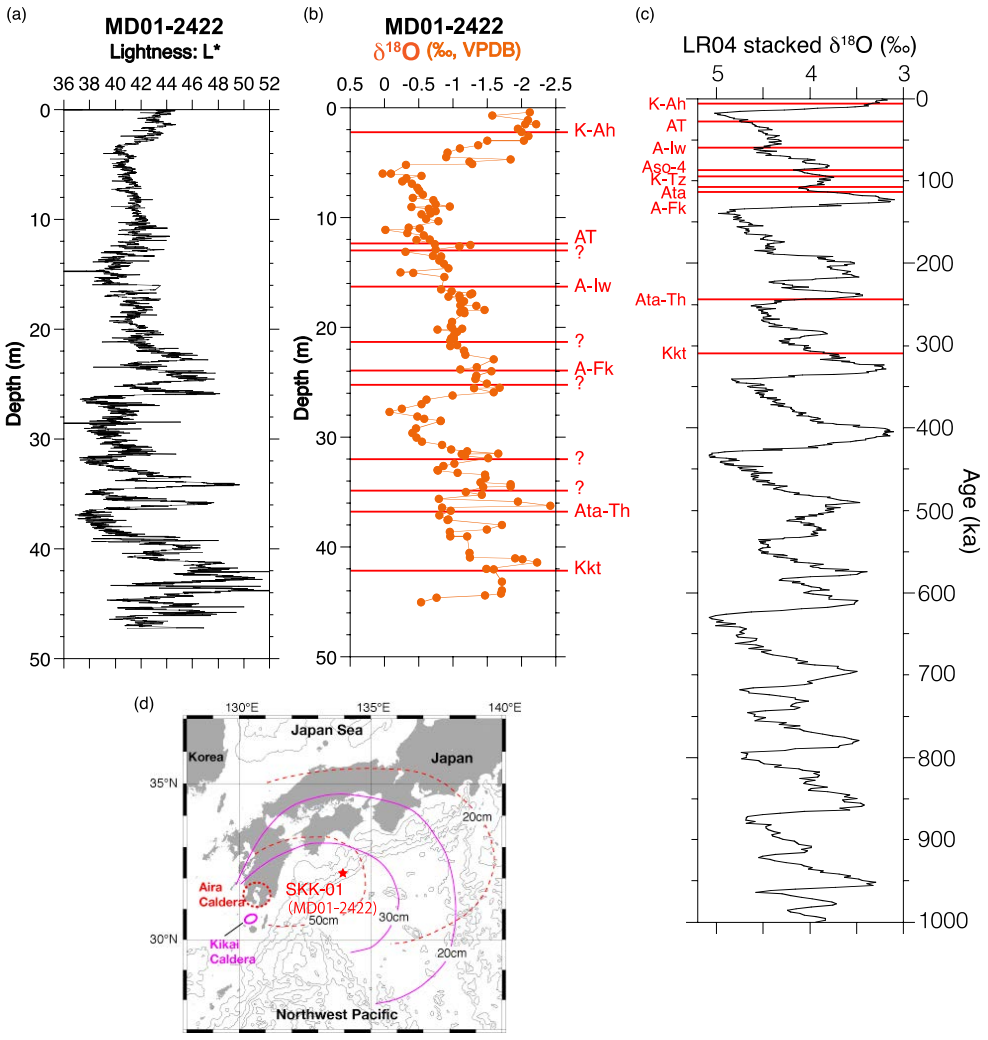

2006). (b) Tephrostratigraphy with $\delta^{18}O$ curve of core MD01-2422 (Ikehara et al., 2006). (c) Composite $\delta^{18}O$ curve with time horizons of major widespread tephra in and around Japan (Machida and Arai, 2003). (d) Map showing the site SKK-01 (MD01-2422) and the location of two caldera volcanos. Isopach contours of tephras Kikai-Akahoya (K-Ah) and Aira-Tn (AT) are shown in red solid and purple dashed lines, respectively (modified from Machida and Arai, 2003).

5. Geological background

Proposed Drilling Site

We proposed a primary drilling site **SKK-02** (32°26.48'N, 134°13.67'E, 2,840 m), and an alternate site **SKK-01** at the location of Core MD01-2422 (32°08.7'N, 133°51.8'E, 2,737 m) on the continental slope off Shikoku (Figs. 4, 5). According to detailed bathymetry map and seismic profiles, **SKK-02** is located within a small basin on the continental slope (Figs. 5, 6). Sediment cores have not been collected at SKK-02, but core MD01-2422 was recovered to 47.3 m depth at SKK-01. Sediments of MD01-2422 are mainly composed of homogeneous silty clay. First age model of MD01-2422 was established from the planktic $\delta^{18}O$ stratigraphy and AMS ^{14}C ages (Ikehara et al., 2006). Averaged sedimentation rate was calculated to be ~12 cm/ka.

The sites **SKK-02** and **SKK-01** are most suitable sites to investigate the detailed variability of the KC. One of the important characteristics of the KC is large meander off Japanese Islands (Kawabe, 1995, Ambe et al., 2004). Kawabe (1995) concluded that the existence of three typical paths of the KC, the nearshore and offshore non-large-meander paths and the typical large-meander path, based on the physical oceanographic observations in the Northwest Pacific. The large-meander is frequently occurred at sough of Japanese Islands, in particular from off Kii Peninsula to off Boso Peninsula. According to the modern observation (1993-2000) of the KC main path, the location of the KC axis is largely varied due to meander in the eastern part of the Shikoku Basin and north of Izu-Ogasawara Ridge (Ambe et al., 2004). However, the KC axis is almost fixed near the proposed sites off Shikoku. Thus, the proposed sites SKK-02 and SKK-01 is good location to detect directly the variation of the KC itself without influences by Kuroshio meander.

In addition, the carbonate preservation is another important advantage for the proposed sites. The main reason for the limitation of long-term and continuous paleoceanographic records in the NW Pacific including the Shikoku Basin is carbonate dissolution. The present lysocline depth in the western Pacific is approximately 3,500 m water depth (Wu and Berger, 1991). Significant dissolutions were occurred during deglaciation steps represented by MIS 7-6, 5-4, and 3-2 in the western equatorial Pacific (Kimoto et al., 2003). In fact, at the piston core PC-08 (~4,000 m water depth) in the northern Shikoku Basin, it was possible to analyze planktic $\delta^{18}O$ in

the last glacial period, but it could not be measured in the last deglaciation and Holocene section (Ikehara et al., 2009). However, the MD01-2422 core (2,737 m water depth) showed the detailed $\delta^{18}O$ variation through the recovered whole sedimentary sequence (Fig. 2a).

ODP sites 1175 and 1176 are drilled at around 3,000 m water depth in the Muroto Transect (Fig. 4b). According to the shipboard analyses, carbonate contents are nearly zero at several analyzed horizons and turbidite layers were recognized in the upper 100 m sequence at both sites (Moore et al., 2001). Because there is no evidence for turbidite layers in core MD01-2422 (Ikehara et al., 2006), we concluded that the proposed sites **SKK-02** and **SKK-01** off Shikoku are the best site for paleoceanographic studies in the NW Pacific.

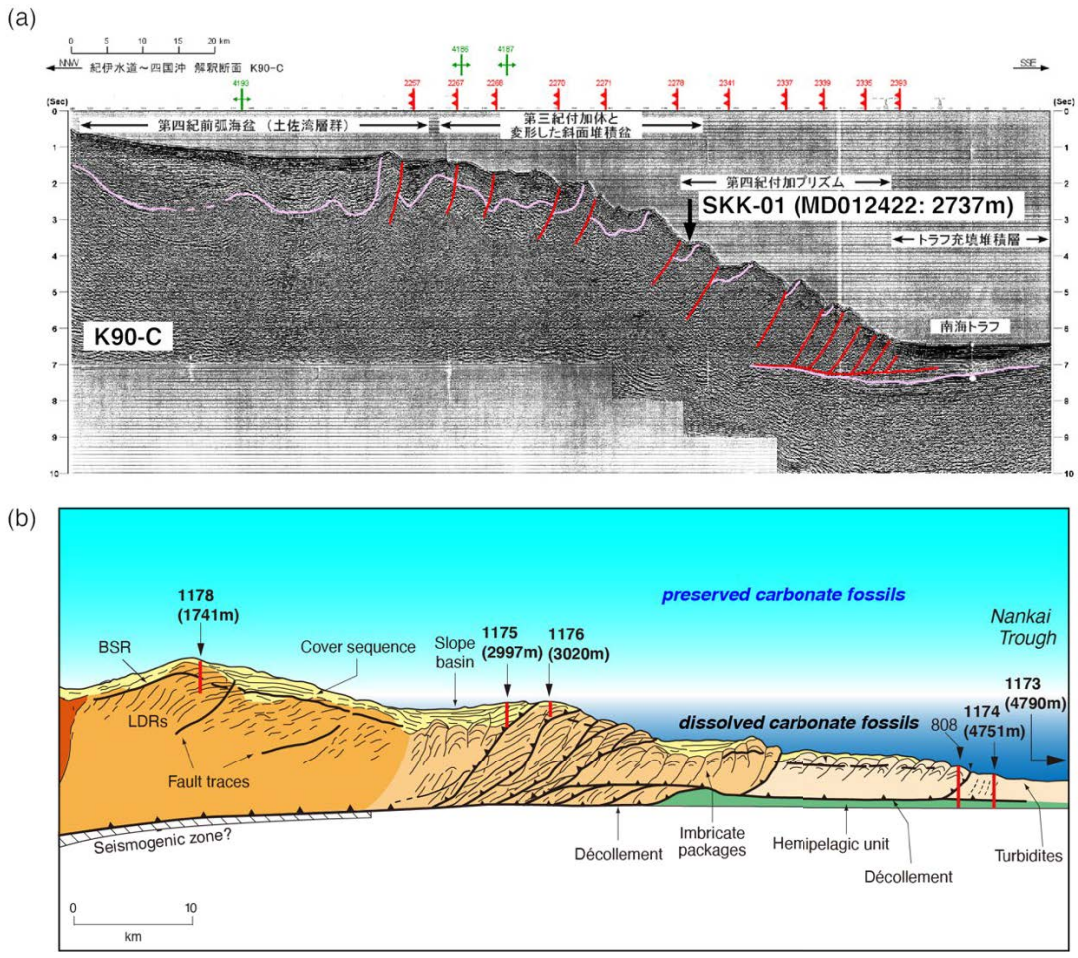

Figure 4. Seismic profile with an alternate proposed site **SKK-01**. (a) Seismic profile of line K90-C on the transect from the Tosa Basin to Nankai Trough (Tokuyama et al., 2001). Site **SKK-01** is located at a small basin on the continental slope. (b) Schematic representation of seismic profile and location of ODP Leg 190 drill sites with carbonate preservation characteristics in seawater (modified after Moore et al., 2001).

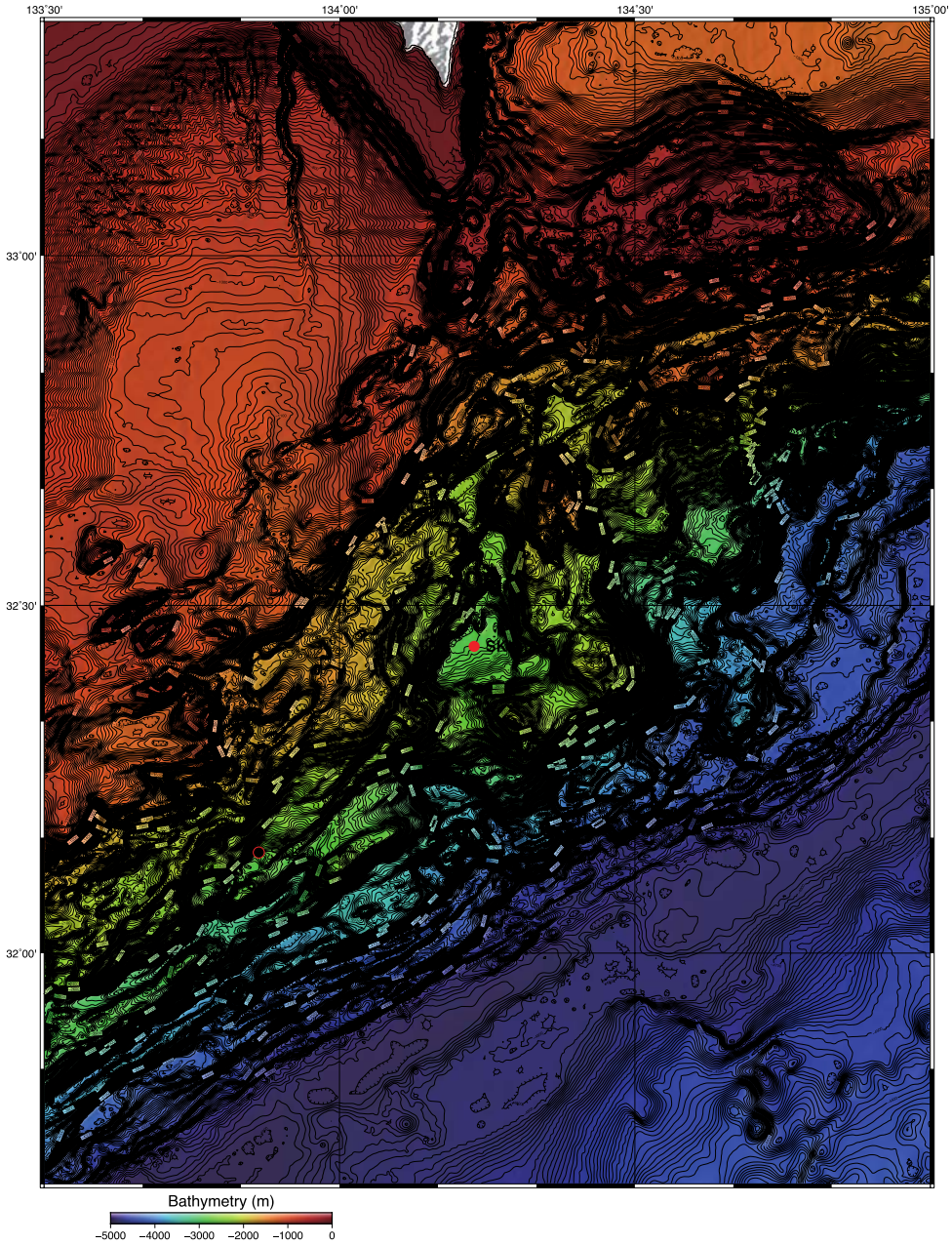

Figure 5. Bathymetric map off Shikoku. Locations of the primary site SKK-02 and alternate site SKK-01 are also shown in the map.

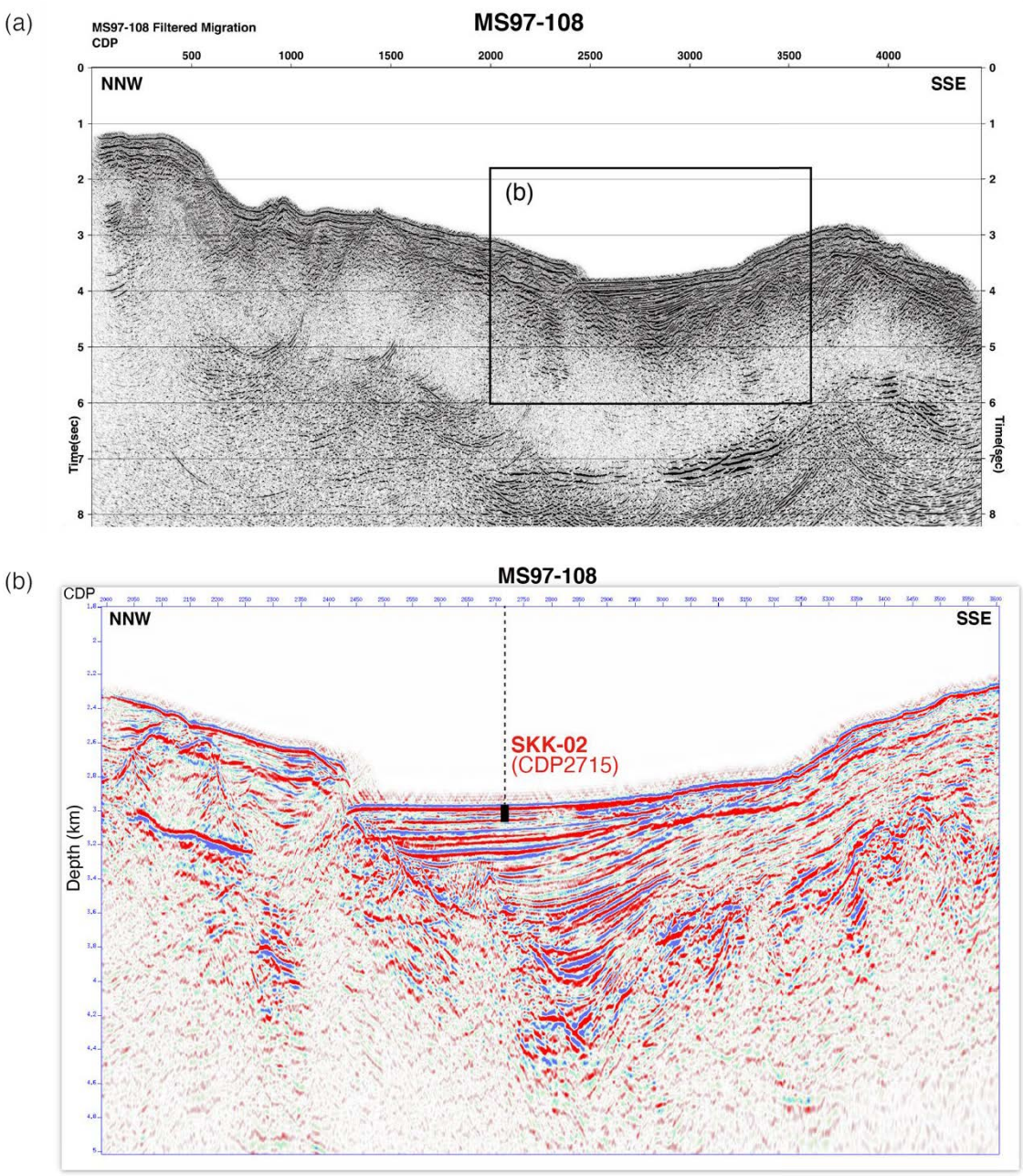

Figure 6. Seismic profile with a primary proposed site **SKK-02**. (a) Seismic profile of line MS97-108 on the transect of continental slope off Shikoku (JAMSTEC, 2004). (b) Closed-up profile of line MS97-108. Site **SKK-02** is located at a small basin on the continental slope.

6. Shipboard core analysis flow

Three holes were drilled for coring at Site C9037 (Table 1). All cores were taken by the Hydraulic Piston Coring System (HPCS) and the short-HPCS (S-HPCS) of D/V Chikyu. The HPCS is designed to take a 9.5-m long core while the S-HPCS is a tool modified from the HPCS to take a shorter core of 4.5 m, 3 m or 1.5 m long. In this expedition, the 3-m type and 4.5-m type S-HPCS was used.

Cores were then used for shipboard sampling and analysis. General core analysis flow is different in each C9037A, C9037B and C9037C. Each flow is shown in Fig. 7, and detailed protocol is described in **9. Method and result of onboard research activities**. Except core sample, we conducted surface water sampling right after arriving at C9037A.

Cores retrieved on the deck were delivered to the Core Cutting Area generally about 30 minutes later after the retrieval. The recovered core length excluding lengths of obvious void spaces were then measured and the Drilling Operations team determined the penetration length (= advance) based on the drilling parameters, the recovered core length and the core condition. A core was cut into 1.4-m long sections and each section length was entered into the J-CORES database, along with core identification information, drilling advance and depth information. At core cutting area, below works were then conducted.

- whole round core (WRC) sampling
- sampling for headspace gas, microbiology, paleontology study

After section cutting and sampling at the core cutting area, sections were then delivered to Core Processing Deck and below laboratory works were conducted.

- X-ray Computed Tomography (X-CT) scanner
- multisensory core logger (MSCL-W)
- PAL sample processing, microscopic observation, smear slide
- WRC sampling
- IW sampling by Rhizon sampler, IW squeezing, sample distribution, pH measurement

・MBIO sampling, sample processing, redox analysis, sample preservation

・surface water sample processing and preservation

・wrap in ESCAL bag after N_2-flush

After expedition, all cores and samples were transported under a cold condition (4℃, -20℃, -40℃) to the Kochi Core Center (KCC) in Kochi, Japan. The personal sampling party of each leg is planned at the KCC sometime after the core transportation.

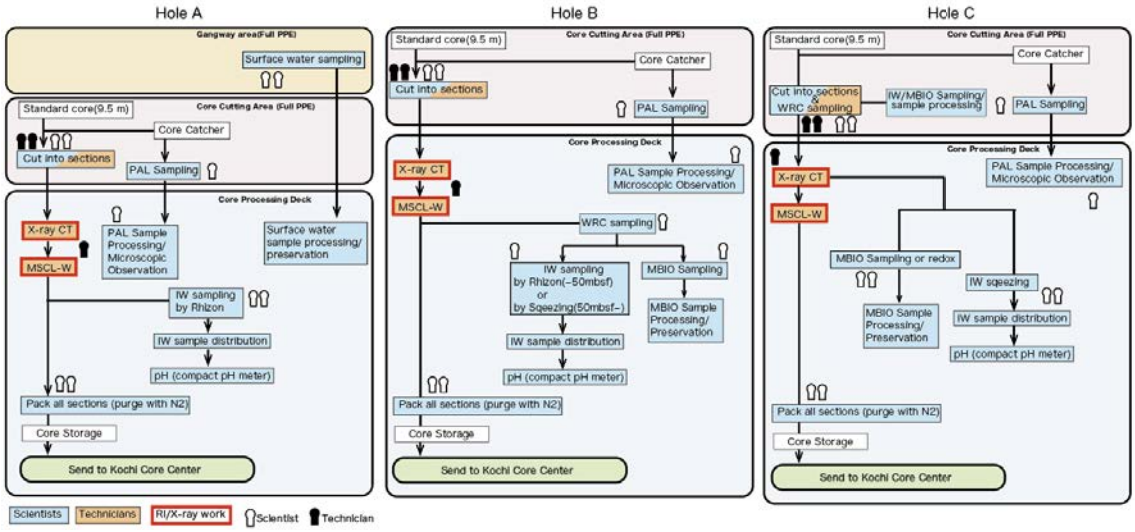

Figure 7. Schematic illustration of shipboard core analysis flow.

Table 1. Hole summary of Site C9037.

Site	Hole	Location		Water Depth	Number of Cores	Total Cored Interval	Inithal Recovery
		Latitude	Longitude	(mMSL)		(m)	(%)
C9037	A	32°26.4800'N	134°13.6700'E	2840.0	11	102.5	111.5
	B	32°26.4839'N	134°13.6745'E	2840.0	12	102.0	111.9
	C	32°26.4761'N	134°13.6655'E	2840.0	13	103.0	105.5

Note: Elevation is 28.5m from mean sea level. End of Hole is the time that vessel left the site location.

7. Operation

The specific operation timetable for this expedition is described in **8. Cruise Log**.
Chikyu SCORE Expedition 913 began on 22th August 2021 when the D/V Chikyu left the port of Shimizu at 9:30. The vessel arrived at the proposed site on 21:00 on 23rd August and we first conducted surface water sampling at 21:20. On the same day, we started making up and running the Hydraulic Piston Coring System (HPCS) assembly without Guide Horn. Shoot for 1H (1st trial) was carried out at 7:58 on 24th from 2832.0 mbsf at C9037A, however, no core was confirmed after on deck at 8:33. Shoot for 1H (2nd trial) and spud-in occurred at 9:35 and we first retrieved core 1H. We observed the mud line and the water depth turned out to be 2840.0 mbsf. Four cores (2H~5H) were then retrieved by the end of the day.

On 25th August, we continued coring and retrieved cores 6H~11H. Table 1 shows each core's depth, advance and recovery. Since the total depth of C9037A reached 102.5 mbsf when the Core 11H was retrieved at 11:06, we moved the vessel to C9037B (10 m northeastward from C9037A) and shot for Core 1H on 17:31. Since the target layer for C9037B was volcanic ash layer expected to be distributed between C9037A-2H and 3H (10~26.5 mbsf) based on C9037A preliminary results, we decided to use S-HPCS for Core 2F and HPCS for 3H in C9037B and cap the ash layer with the mud layer below. We switched the coring system to S-HPCS and retrieved 2F on 22:15. On 26th August, we retrieved 3H~12H and finished coring at C9037B when the Core 12H retrieved at 19:30. The total depth of C9036B was 102.0 mbsf. We then moved the vessel to C9037C (10 m southwestward from C9037A) from 20:20-20:32.

After arriving at C9037C, we shot for 1H at 1:01 on 27th August. During recovering the core, troubleshoot for AFT CLW (core line winch) was occurred because of tangled winding from 1:20-3:14 and then 1H was retrieved at 3:45. After retrieving the core, CLW was changed from AFT to FWD. For the same reason as C9037B, we switched the coring system to S-HPCS and retrieved core at 6:33 and observed no bending of inner barrel. We then continued HPCS coring for 3H~7H. Since the target layer for C9037C was expected to be 68.0-73.5 mbsf based on C9037B preliminary results, we switched the coring system to S-HPCS to make sure to recover the cores and 8F, 9F were retrieved on 28th August. However, the coring gap were also concerned between each S-HPCS cores and it might not suitable for this expedition's scientific objective, we again discussed and decided to switch it back to HPCS before recovering its target layer and conducted HPCS coring from next shoot. Core 10H~11H were then retrieved. After shot for 12H at 10:52 and during recovering, troubleshoot for CLW was occurred because tangled winding was observed even in FWD CLW and then retrieved Core 12H on 15:30. With taking Core 13H, we

terminated the coring operations of this expedition. The total depth of C9037C was 103.0 mbsf. The vessel started sail to Shimizu port at 9:00 on 29th August and the expedition finished with docking of the vessel on 31st August.

Table 2 Summary of each core's advance and recovery.

Core	Type	Depth (mbsf)		Advance	Initial Recovery	
		Top	Bottom	(m)	(m)	(%)
1	H	2.0	10.0	8.0	9.85	123.1
2	H	10.0	17.0	7.0	8.99	128.4
3	H	17.0	26.5	9.5	10.16	106.9
4	H	26.5	36.0	9.5	9.77	102.8
5	H	36.0	45.5	9.5	10.11	106.4
6	H	45.5	55.0	9.5	10.89	114.6
7	H	55.0	64.5	9.5	11.30	118.9
8	H	64.5	74.0	9.5	10.24	107.8
9	H	74.0	83.5	9.5	10.32	108.6
10	H	83.5	93.0	9.5	10.71	112.7
11	H	93.0	102.5	9.5	9.70	102.1
1	H	0.0	6.5	6.5	6.40	98.5
2	F	6.5	11.0	4.5	3.77	83.8
3	H	11.0	20.5	9.5	10.13	106.6
4	H	20.5	30.0	9.5	10.36	109.1
5	H	30.0	39.5	9.5	10.62	111.8
6	H	39.5	49.0	9.5	10.62	111.8
7	H	49.0	58.5	9.5	11.04	116.2
8	H	58.5	68.0	9.5	10.25	107.9
9	H	68.0	73.5	5.5	9.77	177.6
10	H	73.5	83.0	9.5	10.50	110.5
11	H	83.0	92.5	9.5	10.57	111.3
12	H	92.5	102.0	9.5	10.12	106.5
1	H	0.0	6.5	6.5	6.72	103.4
2	F	6.5	10.0	3.5	3.75	107.1
3	H	10.0	19.5	9.5	9.40	98.9
4	H	19.5	29.0	9.5	10.55	111.1
5	H	29.0	38.5	9.5	9.90	104.2
6	H	38.5	48.0	9.5	10.47	110.2
7	H	48.0	57.5	9.5	10.32	108.6
8	F	57.5	60.5	3.0	3.80	126.7
9	F	60.5	65.0	4.5	5.80	128.9
10	H	65.0	74.5	9.5	10.61	111.7
11	H	74.5	84.0	9.5	9.90	104.2
12	H	84.0	93.5	9.5	10.52	110.7
13	H	93.5	103.0	9.5	10.70	112.6

8. Cruise Log

Date	Activity	Plan
22nd Aug	08:00 Embark scientists 09:30 Start sailing to Site SKK-02	Leave port Transit
23rd	00:00 Continue to sail to Site SKK-02 19:30 Arrive at Site SKK-02. Field arrival check and set DP mode 21:00 Surface sea water sampling 22:00 Make up and run 10-5/8" HPCS coring BHA to 437 mBRT.	Transit
24th	00:00 Continue to run the BHA to 2860.5 mBRT while cleaning inside of drill strings with 200 spm x 16.4 MPa 06:45 End running the BHA **Start coring at Hole C9037A** 07:05 Load sinker bar 07:18 Install inner barrel for 1H 07:54 Land inner barrel 07:58 Shoot 1H (1st trial) from 2860.5 mBRT at 16.2 MPa 08:33 Inner barrel on deck and confirm no core 08:50 Install inner barrel for 1H 09:30 Land inner barrel 09:35 Shoot for 1H (2nd trial) from 2870.5 mBRT at 16.8 MPa. Partial penetration. DW assist. Overpull after picking up 1.1 m 10:15 1H core on deck 11:00 Install inner barrel for 2H 11:09 Start washing down to 2878.5 mBRT (8.0 mbsf) w/ 10-30 spm. 12:04 End washing down 12:14 Land inner barrel 12:16 Shoot for 2H at 16.2 MPa. Partial penetration. DW assist. Overpull after picking up 2.5 m 12:30 POOH the BHA above seabed 12:52 2H core on deck 13:17 Start washing down to 2885.5 mBRT (15.0 mbsf) w/ 10-30 spm 13:32 End washing down 15:00 Break out 15:05 Oil burst at RTS while moving AFT for space out 17:00 Resume to space out 17:20 Install inner barrel for 3H 18:34 Land inner barrel 18:37 Shoot for 3H at 16.7 MPa, full stroke 20:30 4H core on deck 20:30 Start washing down to 2904.5 mBRT (34.0 mbsf) w/ 40 spm 21:00 End washing down 21:35 Install inner barrel for 5H 22:00 Land inner barrel 22:05 Shoot for 5H at 16.9 MPa, full stroke. 22:30 5H core on deck 22:45 Start washing down to 2914.0 mBRT (43.5 mbsf) w/ 40 spm 23:00 End washing down 23:45 Install inner barrel for 6H	HPCS
25th	00:29 Land inner barrel 00:32 Shoot for 6H at 16.8 MPa, full stroke. DW assit 1.4 m	

	01:03 6H core on deck 01:09 Start washing and drilling down to 2923.5 mBRT (53.0 mbsf) w/ 40 spm. 01:23 End washing and drilling down 01:42 Install inner barrel for 7H 02:09 Land inner barrel 02:12 Shoot for 7H at 18.0 MPa, full stroke. DW assist 1.9 m. 02:36 7H core on deck 02:39 Start drilling down to 2933.0 mBRT (62.5 mbsf) w/ 40 spm, 20 rpm 03:07 Install inner barrel for 8H 03:40 Land inner barrel 03:43 Shoot for 8H at 17.7 MPa, full stroke. DW assit 0.7 m. 04:10 8H core on deck 04:15 Unload sinker bar 04:31 Start drilling down to 2942.5 mBRT (72.0 mbsf) w/ 40 spm, 20 rpm 04:43 End drilling down 05:05 Load sinker bar 05:17 Install inner barrel for 9H 05:47 Land inner barrel 05:50 Shoot for 9H at 17.2 MPa, full stroke. DW assist 1.5 m. 06:35 9H core on deck 07:09 Start drilling down to 2952.0 mBRT (81.5 mbsf) w/ 40 spm, 20 rpm 07:17 End drilling down 07:34 Install inner barrel for 10 H 08:13 Land inner barrel 08:15 Shoot for 10H at 18.5 MPa, full stroke. DW assist 4 m w/ overpull up to 170 kN. 08:54 10H core on deck 09:13 Start drilling down to 2961.5 mBRT (91.0 mbsf) w/ 40 spm, 20 rpm 09:36 End drilling down 10:25 Land inner barrel 10:27 Shoot for 11H at 19.2 MPa, full stroke. DW assist 5.5 m w/ overpull up to 116 kN 11:06 11H core on deck 11:30 POOH the BHA to 2840.5 mBRT (30 m above seabed) **Finish coring at Hole C9037A** **Start coring at Hole C9037B** 16:00 Run the BHA to 2865.5 mBRT 16:45 Install inner barrel for 1H 17:20 Land inner barrel 17:31 Shoot for 1H at 17.3 MPa, full stroke. 18:18 1H core on deck 18:30 Unload sinker bar. Clean Akema wiper 20:30 Load sinker bar 21:08 Install inner barrel for 2F 21:41 Land inner barrel 21:44 Shoot for 1F at 17.1 MPa, partial penetration. DW assist. Overpull up to 50 kN. 22:15 2F core on deck. Stuck in drill pipe 22:45 Release inner barrel. Bended at ~1.5 m from the top 23:16 Install inner barrel for 3H 23:18 Start washing down to 2877.5 mBRT (9.0 mbsf) w/ 40 spm	
26th	00:00 Continue washing down to 2879.5 mBRT (11.0 mbsf) 00:20 End washing down 00:25 Land inner barrel 00:28 Shoot for 3H at 17.4 PMa, full stroke. 01:03 3H core on deck	HPCS

01:09 Start washing down to 2889.0 mBRT (20.5 mbsf) w/ 40 spm 01:35 End washing down 01:42 Install inner barrel for 4H 02:09 Land inner barrel 02:11 Shoot for 4H at 18.0 MPa, full stroke 02:36 4H core on deck 02:39 Start washing down to 2898.5 mBRT (30 mbsf) w/ 40 spm 02:50 End washing down 02:58 Install inner barrel for 5H 03:25 Land inner barrel 03:28 Shoot for 5H at 17.2 MPa, full stroke. 03:56 5H core on deck 03:58 Start washing down to 2908.0 mBRT (39.5 mbsf) w/ 40 spm 04:08 End washing down 04:45 Unload sinker bar 05:04 Load sinker bar 05:10 Install inner barrel for 6H 05:37 Land inner barrel 05:39 Shoot for 6H at 18.2 MPa, full stroke. 06:28 6H core on deck 06:41 Start washing down to 2918.5 mBRT (49.0 mbsf) w/ 40 spm 07:15 End washing down 07:30 Install inner barrel for 7H 08:03 Land inner barrel 08:07 Shoot for 7H at 18.0 MPa, full stroke. DW assit 5 m w/ overpull up to 85 kN 08:43 7H core on deck 09:02 Start drilling down to 2927.0 mBRT (58.5 mbsf) w/ 40 spm, 10 rpm 09:27 End drilling down 09:45 Install inner barrel for 8H 10:16 Land inner barrel 10:20 Shoot for 8H at 17.3 MPa, full stroke. DW assist 3.5 m w/ overpull upto 150 kN. 10:56 8H core on deck 11:16 Start drilling down to 2936.5 mBRT (68.0 mbsf) w/ 40 spm, 10-20 rpm 11:45 Install inner barrel for 9H 12:17 Land inner barrel 12:19 Shoot for 9H at 19.5 MPa, partial penetration. DW assist 4 m w/ overpull up to 60 kN 13:00 9H core on deck 13:20 Unload sinker bar 14:05 Load sinker bar 13:30 Start drilling down to 2942.0 mBRT (73.5 mbsf) w/ 40 spm, 10-20 rpm 13:55 End drilling down 14:45 Install inner barrel for 10H 15:25 Land inner barrel 15:30 Shoot for 10H at 17.5 MPa, full stroke. DW assist 1.5 m w/ overpull up to 170 kN 16:00 10H core on deck 16:05 Start drilling down to 2951.5 mBRT (83.0 mbsf) w/ 40 spm, 10-20 rpm 16:32 End drilling down 16:40 Install inner barrel for 11H 17:15 Land inner barrel 17:17 Shoot for 11H at 17.7 MPa, full stroke. DW assist 1.5 m w/ overpull up to 50 kN 17:46 11H core on deck 18:00 Start drilling down to 2961.0 mBRT (92.5 mbsf) w/ 40 spm, 10-20 rpm 18:15 End drilling down	

	19:00 Land inner barrel 19:03 Shoot for 12H at 16.8 MPa, full stroke. DW assist 4.5 m w/ 40 spm, 10-20 rpm 19:30 12H core on deck 19:45 POOH to 2830.0 mBRT (38.5 m above seabed) **Finish coring at Hole C9037B** 20:15 Rig services **Start coring at Hole C9083C** 23:45 Start running the BHA	
27th	00:00 Continue to run the BHA to 2865.5 mBRT 00:14 Load sinker bar 00:24 Install inner barrel for 1H 00:58 Land inner barrel 01:01 Shoot for 1H at 17.3 MPa, full stroke 01:20 Trouble shoot for core line winch (CLW): tangled winding 03:14 Resume operation 03:45 1H core on deck 03:53 Unload sinker bar 04:05 Change CLW from AFT to FWD 04:20 Resume operation, load sinker bar 04:36 Install inner barrel for 2F 04:39 Start washing down to 2875.0 mBRT (6.5 mbsf) w/ 40 spm 05:00 End washing down 05:22 Land inner barrel 05:24 Shoot for 2F at 18.5 MPa, partial penetration. DW assist w/ overpull up to 30 kN after picking up 1.6 m 06:33 2F core on deck 06:36 Install inner barrel for 3H 07:15 Start washing down to 2878.5 mBRT (10.0 mbsf) w/ 20 spm 08:03 End washing down 08:28 Land inner barrel 08:30 Shoot for 3H at 19.2 MPa, full penetration. DW assist 7.5 m w/ overpull up to 70 kN 09:20 3H core on deck 09:52 Start washing down to 2888.0 mBRT (19.5 mbsf) w/ 20 spm 10:24 End washing down 10:43 Install inner barrel for 4H 11:30 Land inner barrel 11:32 Shoot for 4H at 17.3 MPa, full stroke 12:18 4H core on deck 12:22 Start washing down to 2897.5 mBRT (29.0 mbsf) w/ 20 spm 12:50 End washing down 13:00 Install inner barrel for 5H 14:46 Land inner barrel 14:48 Shoot for 5H at 18.3 MPa, full penetration. DW assist w/ 10 kN 14:40 5H core on deck 14:45 Unload sinker bar 15:05 Start washing down to 2904.0 mBRT (35.5 mbsf) w/ 30 spm 15:30 End washing down for lay out, found oil leak at Hydraulic Elevator 15:45 Maintenance Hydraulic Elevator 16:50 Resume washing down to 2907.0 mBRT (38.5 mbsf) w/ 30 spm 17:10 End washing down, load sinker bar 17:40 Install inner barrel for 6H	HPCS

	18:28 Land inner barrel 18:30 Shoot for 6H at 16.8 MPa, full stroke 19:22 6H core on deck 19:25 Start drilling down to 2916.5 mBRT (48.0 mbsf) w/ 30-40 spm, 20 rpm 19:50 End drilling down 20;00 Install inner barrel for 7H 21:12 Land inner barrel 21:13 Shoot for 7H at 18.3 MPa, full stroke 22:05 7H core on deck 22:24 Start drilling down to 2926.0 mBRT (57.5 mbsf) w/ 40 spm, 20 rpm 22:43 End drilling down 22:50 Install inner barrel (3 m) for 8F 23:30 Land inner barrel 23:31 Shoot for 8F at 18.9 MPa, full stroke. DW assist w/ overpull up to 70 kN	
28th	00:21 8F core on deck 00:28 Start drilling down to 2929.0 mBRT (60.6 mbsf) w/ 40 spm, 20 rpm 00:45 Install inner barrel (4.5 m) for 9F 01:25 Land inner barrel 01]27 Shoot for 9F at 18.9 MPa, full stroke. DW assist 2 m w/ overpull up to 150 kN 02:11 9F core on deck 02:17 Start drilling down to 2933.5 mBRT (65 mbsf) w/ 40 spm, 20 rpm 02:26 End drilling down 02:35 Unload sinker bar 02:45 Clean up Akema wiper and pipe connection 03:25 Attempt to load sinker bar, but fail due to sick grease 04:00 Clean up sinker bar and Akema wiper 04:55 Resume operation, load sinker bar 05:02 Install inner barrel for 10H 05:44 Land inner barrel 05:46 Shoot for 10H at 18.4 MPa, full stroke. DW assist 4.5 m w/ overpull up to 130 kN 06:58 10H core on deck 07:15 Start drilling down to 2943.0 mBRT (74.5 mbsf) w/ 40 spm, 20 rpm 07:36 End drilling down 07:54 Install inner barrel for 11H 08:38 Land inner barrel 08:40 Shoot for 11H at 17.2 MPa, full stroke. DW assist 5.5 m w/ overpull up to 130 kN 09:30 11H core on deck 09:39 Start drilling down to 2952.0 mBRT (84.0 mbsf) w/ 40 spm, 20 rpm 09:55 End drilling down 10:08 Install inner barrel for 12H 10:48 Land inner barrel 10:52 Shoot for 12H at 18.5 MPa, full stroke. DW assist 7 m w/ overpull up to 75 kN 10:55 Start retrieving inner barrel to 370 m 11:36 Trouble shoot for CLW: tangled winding. Payout CLW to 2500 m 14:00 Resume retrieving inner barrel to surface 15:30 12H core on deck 15:40 Start drilling down to 2962.0 mBRT (93.5 mbsf) w/ 40 spm, 20 rpm 16:10 End drilling down 16:25 Install inner barrel for 13H 17:20 Land inner barrel 17:21 Shoot for 13H at 17.8 MPa, full stroke. DW assist 7.5 m w/ overpull up to 90 kN 19:12 13H core on deck 19:20 Unload sinker bar 19:30 POOH the BHA to 2770.0 mBRT	HPCS

	Finish coring at Hole C9037 20:30 Load and run sinker bar for CLW maintenance	
29th	00:00 Continue maintenance 01:00 POOH the BHA to surface while flushing inside of drill strings 10:30 Start sailing to Shimizu port	HPCS
30th	Continue to sail to Shimizu port	HPCS Transit
31st	09:00 Pilot onboard 10:30 Arrive at Shimizu port 11:00 Disembark scientist End of cruise	End of cruise

9. Method and result of onboard research activities

9.1. X-ray computed tomography

X-ray CT images were done immediately after dividing the core into sections and were used to identify 3-D sedimentary and structural features, such as bioturbation burrows, bedding planes, gas void, and so on. The X-ray CT images also performs the preliminary assessment of core quality through imaging destruction of geological features and drilling disturbance.

Method

Our methods followed those in the measurement manual prepared by Institute for Marine-Earth Exploration and Engineering (MarE3) (3D X-ray CT Scanning, Version 3.00; 24 March 2015). The X-ray CT instrument on the Chikyu is a Discovery CT 750HD (GE Medical Systems) capable of generating thirty-two 0.625 mm thick slice images every 0.4 s, the time for one revolution of the X17 ray source around the sample. Data generated for each core consist of core-axis-normal planes of X-ray attenuation values with dimensions of 512 Å~ 512 pixels. Data were stored on the server as Digital Imaging and Communication in Medicine (DICOM) formatted files. The DICOM files were restructured to create 3-D images for further investigation. The theory behind X-ray CT has been well established through medical research and is very briefly outlined here. X-ray intensity varies as a function of X-ray path length and the linear attenuation coefficient (LAC) of the target material:

$I = I0 Å\sim e{-}\mu L,$

where
I = transmitted X-ray intensity,
I0 = initial X-ray intensity,
μ = LAC of the target material, and
L = X-ray path length through the material.
LAC is a physical index about the X-ray beam reduction during translation of target materials. LAC is led from the relationship be- tween physical properties of target materials (i.e., chemical composition, density, and state). The basic measure of attenuation, or radiodensity, is the CT number given in Hounsfield units (HU):

$CT\ number = [(\mu t - \mu w)/\mu w] Å\sim 1000,$

where

μt = LAC for the target material, and
μw = LAC for water.

The distribution of attenuation values mapped to an individual slice comprises the raw data that are used for subsequent image processing. Successive 2-D slices yield a representation of attenuation values in 3-D pixels referred to as voxels. Analytical standards used during Expedition 370 were air (CT number = −1000), water (CT number = 0), and aluminum (2477 < CT number < 2487) in an acrylic core mock-up. All three standards were run once daily after air calibration. For each standard analysis, the CT number was determined for a 24.85 mm^2 area at fixed coordinates near the center of the cylinder.

Preliminary Results

The X-ray CT instrument worked well enough to obtain X-ray CT images for our investigation. One example of the X-ray CT image is shown in Fig. 8. Based on the CT image of C9037B, a thick layer of volcanic glass with a thickness of about 7 m was observed from C9037B-1H-CC to C9037B-3H-2. Many turbidite layers were also observed in the entire cores of each holes.

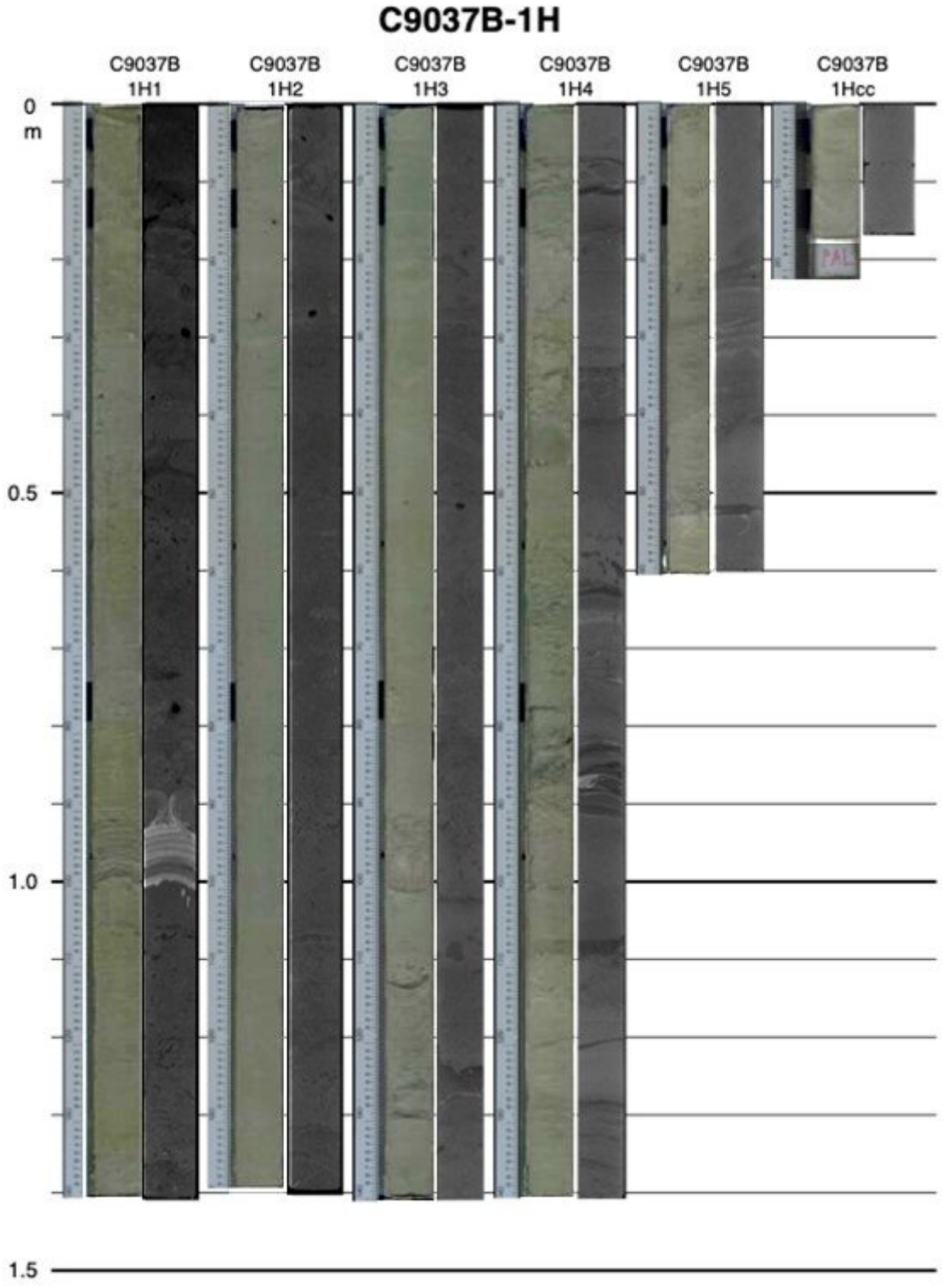

Figure 8. Examples of core photograph (left) and X-ray CT image (right) of the drilled core at C9037 off Shikoku.

9.2. Physical properties measurements of whole-round core with the Multi-Sensor-Core-Logger

All physical property measurements were conducted after the X-ray CT images were taken. The MSCL-W (GeoTek Ltd., London, United Kingdom) allows nondestructive measurements on whole-round core (WRC) samples including gamma ray attenuation (GRA) density, ultrasonic P-wave velocity (VP), noncontact electrical resistivity (NCR), and magnetic susceptibility (MS).

Method

Gamma ray attenuation (GRA) density: Bulk density is used to evaluate pore volume in sediment, which provides information on the consolidation state. GRA is based on the detection of a gamma ray beam during its passage through the sediment. The beam, produced by a 370 MBq ^{137}Cs gamma ray source within a lead shield with a 5 mm collimator, was directed through WRCs. The gamma ray detector includes a scintillator and an integral photomultiplier tube to record the gamma rays that pass through the WRC. GRA bulk density (ρ_b) was calculated as

$\rho_b = \ln(I_0/I)/\mu d$,

where

I_0 = gamma ray source intensity,

I = measured intensity of gamma rays passing through the sample,

μ = Compton attenuation coefficient, and

d = sample diameter.

The Compton attenuation coefficient (μ) and source intensity (I_0) were treated as constants, so ρ_b can be calculated from I. The gamma ray detector was calibrated with a sealed calibration core (a standard core liner filled with distilled water and aluminum cylinders of various diameters). To establish the calibration curves, gamma ray counts were measured through a 7 cm diameter standard cylinder composed of aluminum with six different diameters (1–6 cm) (density = 2.7 g/cm^3) filled with surrounding relationship between I and μd is

$\ln(I) = A(\mu d) + B$,

where A and B are coefficients determined from the calibration experiment. GRA density measurements on core samples were conducted every 4 cm for 4 s. The spatial resolution is 5 mm.

Ultrasonic P-wave velocity: Ultrasonic P-wave velocity (VP) was measured for WR cores by measuring sonde length (d) (outer liner diameter) and travel time (t_0):

$VP = d/t_0$.

A linear variable differential transformer, used to measure the liner thickness, is integrated with a 230 kHz P-wave transmitter/receiver system. The system is mounted horizontally on the MSCLW
system and measures d and t_0 perpendicular to the core axis at 4 cm intervals. The measured travel
time (t0) between the transducers is delayed by the pulse travel time through the liner, the threshold
peak detection procedure, and the pulse travel between transducers and the electronic circuitry. Travel time is corrected for these parameters by calibrating the system using a core liner filled with pure water, which has a known P-wave velocity (1480 m/s at 20°C). The corrected P-wave velocity through the core (Vcore) (m/s) is

$$Vcore = (d - W)/[t0 - tw - (d - W)/Vw],$$

where

W = total wall thickness of the core liner,

tw = measured travel time through the water-filled calibration liner, and

Vw = known P-wave velocity of pure water at room temperature.

Noncontact electrical resistivity (NCR): Within limits, electrical resistivity may be useful for estimating other sediment physical properties, including porosity, tortuosity, permeability, and thermal conductivity. Bulk electrical resistivity is controlled by solid grain resistivity, interstitial water resistivity, pore space distribution, and pore connectivity. Electrical resistivity (ρ) is defined by the electrical resistance and geometry of the core measured:

$$\rho=R(A/L)$$

where R = electrical resistance, L = length of measurement, and A = cross-sectional area of the core. The noncontact resistivity sensor on the MSCL-W system induces a high-frequency magnetic field in the core with a transmitter coil. This generates an electrical current in the bulk sediment that is inversely proportional to its resistivity. The secondary magnetic field generated by this induced electrical current is measured by a receiver coil. To measure this smaller magnetic field accurately, a differencing technique has been developed that compares readings from the sample core to readings from an identical set of coils operating in air. Electrical resistivity data were obtained at 4 cm intervals on the MSCL-W.

Magnetic susceptibility (MS): MS is the degree to which a material can be magnetized by an external magnetic field. Therefore, MS reflects the composition of sediment. An 8 cm diameter Bartington loop sensor was used to measure MS. An oscillator circuit in the sensor produces a low-intensity (~80 A/m root-mean-square) nonsaturating alternating magnetic field (0.565 kHz).

This pulse frequency was converted into MS. The spatial resolution of the loop sensor is 23–27 mm. MS data were collected every 1 cm along the core.

Results

Physical properties (GRA, VP, NCR, and MS) measured by the MSCL-W instrument were properly obtained. Since some cores have cracks, gas voids, and water, downcore data of GRA, VP, and NCR show very high frequency fluctuations. MS records from three holes show similar change, suggesting the potential of inter-hole correlation.

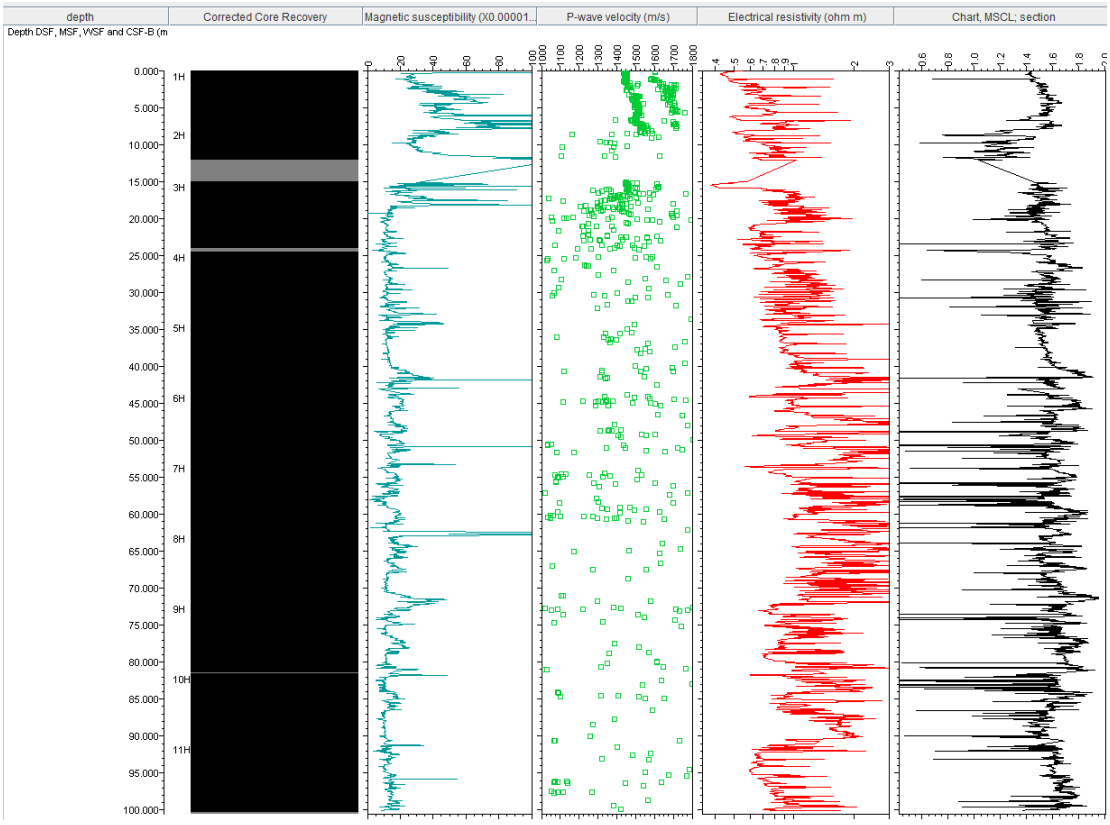

Figure 9. Down-core results of physical properties of Hole C9037A measured by the MSCL-W.

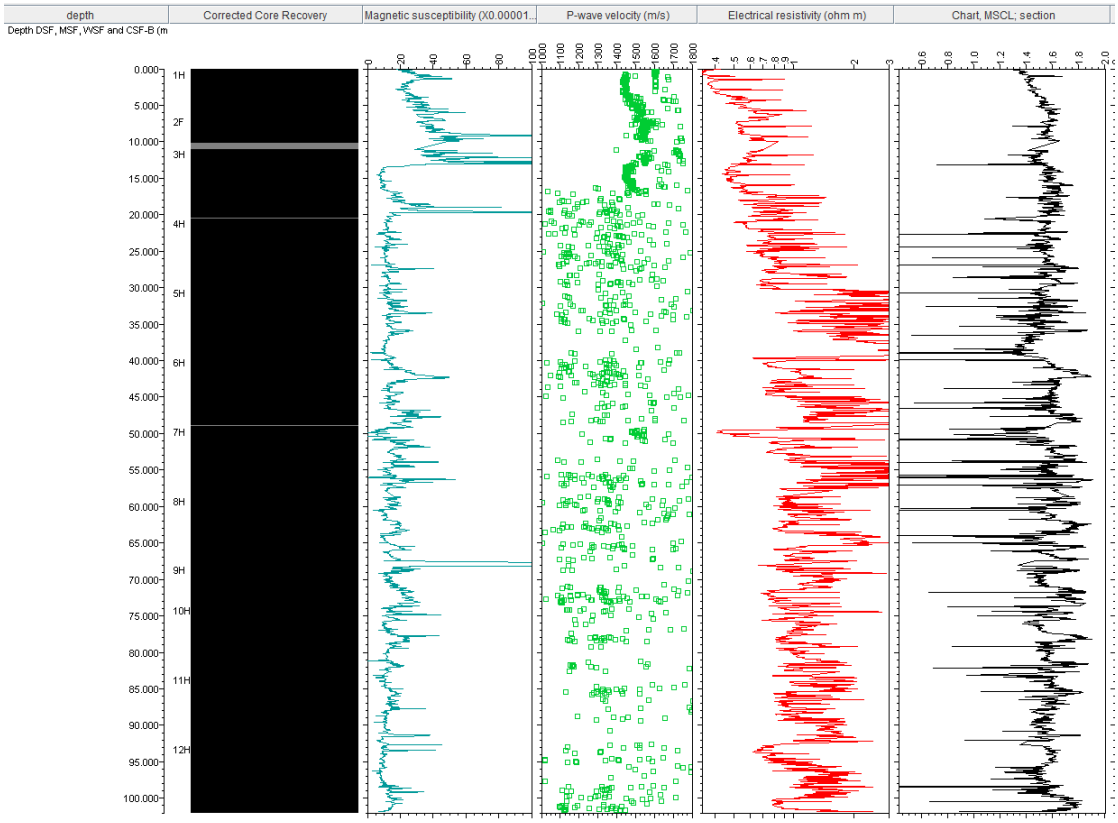

Figure 10. Down-core results of physical properties of Hole C9037B measured by the MSCL-W.

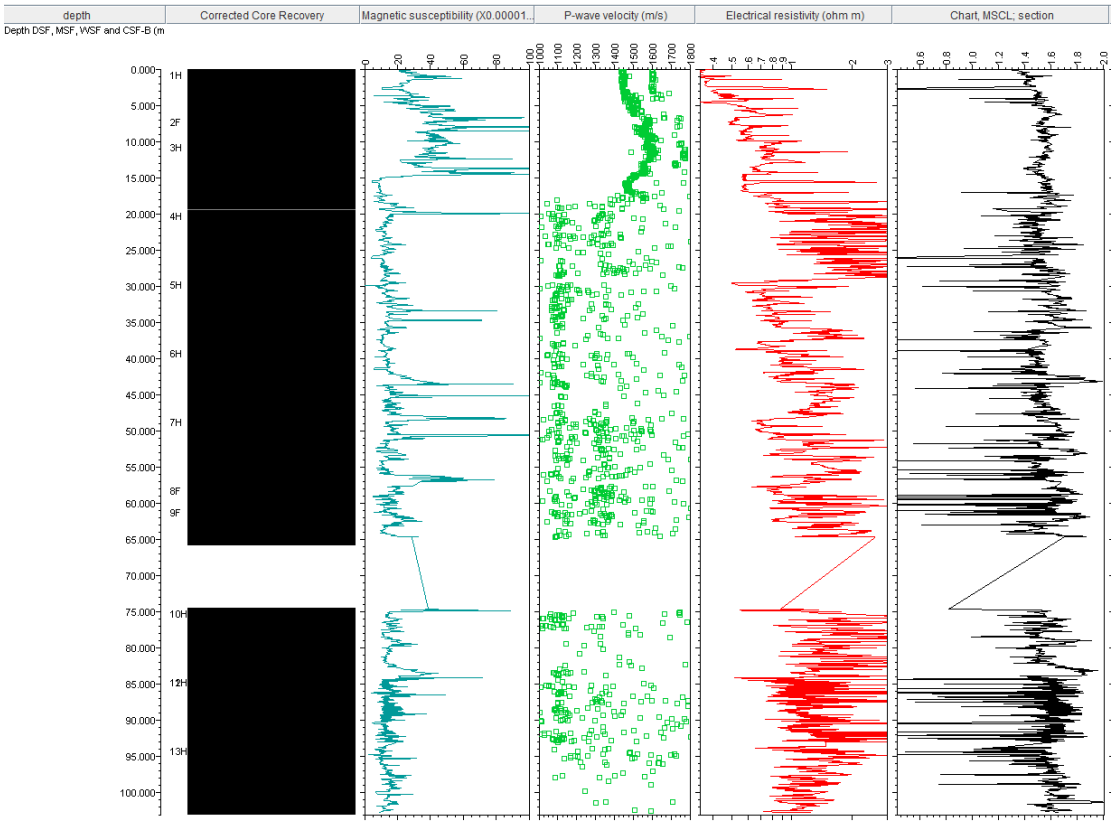

Figure 11. Down-core results of physical properties of Hole C9037C measured by the MSCL-W. (The depth information in the lower part of the core is wrong in J-CORES, and the plot needs to be corrected.)

9.3. Micropaleontology

9.3.1 Radiolaria

We proceeded 10 sediment core catcher samples from Holes A to C respectively, to determine preliminary radiolarian biostratigraphy at Site C9037. The used sample correspond approximately to the lowest 5 cm of each core catcher. The samples were treated with hydrogen peroxide (10%) and hydrochloric acid (5%) to remove organic and calcareous matter. The sediment reacted with the chemical for 10 minutes. Undissolved residues were sieved over a 45-µm screen and were dried on a slide, mounted with Norland optical adhesive, and covered with a 24 mm × 40 mm cover glass for microscopic analysis. The adhesive was solidified by placing the slide under UV light for ~10 min. For each sample more than 1000 specimens were observed for identify biostratigraphic species and then 200 to 300 radiolarian species were counted randomly for monitor preliminary changes in radiolarian assemblages under a Zweis binocular microscope. Slides were examined at 50× to 400× for stratigraphic markers and other common taxa following Matsuzaki et al. (2014, 2015) nomenclature using a Zeiss microscope.

Relative abundances are estimated for estimate the evolution of radiolarian assemblages (See Appendix 1), and Radiolarian abundances is estimated as follows:

A=more than 1000 skeletons in a slide

C=between 500-1000 skeletons in a slide

F=between 100 and 500 skeletons in a slide

R=between 10 and 100 skeletons in a slide

B= less than 10 skeletons a slide.

The radiolarian biostratigraphic scheme used during Expedition 913 is described in Matsuzaki et al. (2014, 2015) and was established for the area off Kii Peninsula near Site C9037 and thus is suitable for this study. Matsuzaki et al. (2014, 2015) indicated three radiolarian bio-event can be used for the Brunhes/Matuyama chron interval. The Last Occurrence (LO) of *Stylatractus universus* Hays (460±40ka), the First Occurrence (FO) of *Actinomma archadophorum* Haeckel (640±40ka) and LO of *Eucyrtidium matuyamai* Hays (10504±50ka). The age of each datums were assigned from Matsuzaki et al. (2014, 2015), which calibrated each datum to the oxygen isotope stratigraphy tuned to the LR04. For the case of *Stylatractus universus*, Matsuzaki (2021) rename this species as *Xiphosphaerantha angelina* (Campbell and Clark) sensu Sugiyama because of taxonomic legacy issues. The revised name is used herein.

The sample materials analyzed from Hole A to Hole C showed sustained reworkings of sediments. Indeed, at samples Hole A 2H-CC the Pliocene species *Thecosphaera akitaensis* Nakaseko were encountered, while at sample Hole A 5H-CC and 11H-CC, *Eucyrtidium matuyamai* Hays spanning from 1800 to 1050 Ma (Matszuzaki et al., 2014) is mixed with fauna only occurring between 600 and 0 ka such as *Actinomma archadophorum* Haeckel (Matsuzaki et al., 2014). Therefore, we consider it is due to sediment reworkings. At Hole B and Hole C radiolarian fauna suggest less intense reworking but some samples are moderately reworked as well. In addition, no biostratigraphic index were encountered in the analyzed 11 core catcher samples, thus, we assume sediments to be younger than 450 ka. Lastly, estimates of changes in relative abundances of subtropical and coastal fauna (ie., *Lithomelissa setosa* Jörgensen) shows cyclic variation varying from 20 to 55% and from 2 to 8% respectively (Appendix 1). Considering mirror relationship in the fluctuation pattern in coastal and subtropical species relative abundances (mainly composed of *Tetrapyle Cirlcularis/fruticos*a group and *Phorticium polycladum*), it is possible that both curves' fluctuations pattern infers glacial/interglacial periods. If correct, radiolarian fauna suggest that the bottom of the retrieved cores correspond roughly to the middle of Marine Isotopic Stage (MIS) 8.

9.3.2 Calcareous nannofossils

In this study, we investigated changes in calcareous nannofossils assemblages for 30 sediment core catcher samples from Holes C9037 Hole A to C for establish a preliminary depth age model. We prepared smear slide following the nomenclature of Bown and Young (1998). Then, calcareous nannofossils were observed at 1500× magnification using the Zeiss binocular microscope. At least 200 nannofossil specimens were identified, and the nannofossil abundance for each sample was evaluated the nomenclature of following Chiyonobu et al. (2017): A (very abundant) = more than 50 specimens per field of view (FOV); C (common) = 10 to 50 specimens per FOV; R (rare) = 1 to 10 specimens per one to two FOV; and P (present) = one specimen per more three FOV. In addition, we conducted three transects on the smear slide to recognize possible the nannofossil biohorizons. In particular we pay attention of the FO of *Emiliania huxleyi* (290 ka; Anthonissen and Ogg, 2012) and the LO of *Pseudoemiliania lacunosa* (440 ka; Anthonissen and Ogg, 2012).

The nannofossils preservation state was reported following the criteria of Kuwano et al. (2021): G = good, most nannofossil specimens showed little or no sign of dissolution and/or overgrowth; M = moderate, nannofossil specimens showed slightly etching and/or overgrowth, but still identifiable; P = poor, most of the specimens exhibited severe etching and/or overgrowth and hampering proper identification.

For the taxonomy, we followed Young (1998) and Young et al. (2017) nomenclature, but the genus *Gephyrocapsa* was subdivided into three groups based on Backman et al. (2012): large *Gephyrocapsa* spp. (>5.5 μm in length), medium *Gephyrocapsa* spp. (4–5.5 μm), and small *Gephyrocapsa* spp. (<4 μm).

A total of 36 core catcher samples were obtained from C9037A to C9037C. In general, the observed samples were abundant in calcareous nannofossils, however the preservations of specimens were moderate. At least 30 species belonging to 21 genera were identified in the Site C9037 (Appendix 2). Three taxa generally dominating Pleistocene flora were observed such as *Emiliania huxleyi*, *Gephyrocapsa* spp., *Florisphaera profunda*. These spices were dominant throughout the studied samples. In addition, reworked specimens, such as *Pseudoemiliania lacunosa*, *Reticulofenestra asanoi*, *Discoaster* spp., *Sphenolithus* spp., suggesting that samples to be older than mid Pleistocene were often observed in samples from the Site C9037. However, *Emiliania huxleyi* was continuously observed in all analyzed samples, thus the examined sections were estimated to be younger than 290 ka.

9.3.3 Planktic Foraminifera

We analysed 20 cc of core catcher sediment retrieved from Hole A to C, for 30 samples. These sediments were wet sieved through a 63 μm sieve and dried in oven at 40°C. After drying,

planktic foraminifers were sieved again with a >125 μm size fraction and identified to the species level following Schiebel and Hemleben (2017) and Saito et al. (1981) for modern planktic foraminifers. Planktic foraminifers were picked up using a fine brush. For important biostratigraphic marker for the last 1 Ma, we referred to Kucera and Kennett (2000), Domitsu and Oda (2008), and Hayashi et al. (2011). The possible biostratigraphic datum are as follows: last occurrence (LO) of *Globigerinoides ruber* (pink) (120 ka), LO of *Truncorotalia tosaensis* (610 ka), LO of *Neogloboquadrina inglei* (730 ka), and first occurrence (FO) of *Truncorotalia classaformis hessi* (800 ka). At Site C9037, the planktic foraminiferal zonation established for the Northwest Pacific offshore Japan by Domitsu et al. (2011) and Hayashi et al. (2011) was applied.

Faunal counts for semi quantitative estimate were conducted and summarized in the results table (Appendix 3) using the following nomenclature (abundant (A): >16%, common (C): 8%–16%, rare (R): 4%–8%, present (P): <4%) for all samples containing >100 specimens. For samples with less than 100 specimens, we used "+" in the data tables for document species occurences.

No planktic foraminiferal zonation was identified except that 1 specimen of *G. ruber* (pink) was found in sample C9037B-12H-CC. The presence of *G. ruber* (pink) in the lowest part of Hole B suggests that this section is at least older than the LO of *G. ruber* (pink), which is defined at 120 ka. Planktic foraminifer microfossils preservations were not good with mineral coating and many tests were fragmented. Samples in 1H and 2H (2F) of each hole, volcanic ash were abundant, and samples were barren in biogenic fossils. Results of selected foraminiferal assemblages were given in Appendix 3. Even though small planktic foraminifers were dominant because of sieving with a 125 μm sieve, cosmopolitan species were abundant in the assemblages. The relative abundance of species related tropical to subtropical genus such as *Globigerinoides*, *Globoturborotalita*, and *Globorotalia* seemed to fluctuate periodically with peaks in 3H and 10H in Hole B and 3H, 8F, and 10H in Hole C. The fluctuation pattern of relative abundances of warm tropical to subtropical taxa nearly in each hole were almost synchronous.

9.4. Geochemistry

9.4.1 Extraction of interstitial water

From Hole A, the interstitial water was extracted using Rhizon fluid sampler of 10 mL. A 4 mm hole was made with an electric drill on the cap of the section top, and the needle of Rhizon sampler was stuck from the hole. The samples were collected from every section from Core 1H to 4H, every two sections from Core 5H and 6H, and every three sections from Core 7H to 11H, in the cold room at 4 °C. Total 39 samples were collected.

From Hole B, the interstitial water was collected from two sand layers and one ash layer

using Rhizon fluid sampler. These layers were cut to 5–7 cm-long sections, and water was extracted from the sub-sections by sticking the needle of Rhizon sampler into cut surface. Five samples were collected from the ash layer in Core 3H-7. Six and five samples were collected from the sand layers in Core 5H-6 and Core 10H-3, respectively.

From Hole C, the interstitial water was extracted by using a titanium squeezer. A 5 cm-long WRC sample was collected for interstitial water extraction immediately after X-ray CT observation. The WRC samples were taken from every core except for Core 2. The collected WRCs were transferred into a N_2-filled glove bag and pushed out from the plastic core liner. The surface of the sediments was carefully removed to avoid any contamination and/or disturbance with core liner. The interstitial water was extracted from the trimmed sediment core using hydraulic squeezing system onboard (90 mm ø) with a pressure up to 40 MPa into the pre-washed plastic syringe following the standard IODP/Chikyu protocol. Only from the top of Core 1H-1, the interstitial water was collected using Rhizon fluid sampler. Total 10 samples were collected from Hole C. The interstitial water was sub-sampled through the 0.45 μm disposable disk filter for onshore.

9.4.2 Sub-sampling

The interstitial water samples were sub-sampled through the 0.45 μm disposable disk filter for onshore analyses of dissolved organic matter, dissolved inorganic carbon, δ^{18}O-D/H, and major/minor elementals using IC, ICP-MS, and ICP-AES.

9.4.3 pH analysis

pH was analyzed using a pH meter (LAQUAtwin, HORIBA Advanced Techno, Co., Ltd.). About 0.2 mL of water was used for the analysis. Figure 12 shows the vertical profiles of pH from Hole A, B, and C. In Holes A and C, pH was increased from 7.5 at 0 m to 7.9 at 9.2 m with increasing depth, then decrease to 7.5 at 17.7 m. Below 17.7 m, pH was scattered and varied from 7.4 and 7.9, but generally decrease to 7.4 at 77.4 m. Between 90.3 and 100 m, pH varied from 7.5 to 7.8. In the samples obtained from sand and ash layers in Hole C, the pH values varied from 7.6 to 8.1, and were higher than those in Hole A and C.

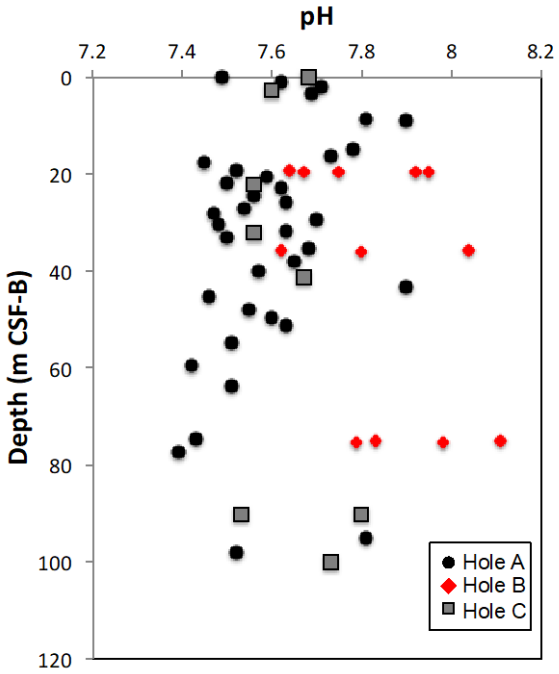

Figure 12. Vertical profiles of pH in Hole A, B, and C.

9.4.4 Headspace gas sample

The headspace gas sample was collected from WRC samples in Hole B and Hole C, which were collected for the interstitial water extraction. A 2.5 cm^3 sediment was collected with a cut-off plastic syringe from the cut surface of WRC sample, and was extruded into a 24 mL glass vial and immediately sealed with a butyl- rubber septum and metal crimp cap. The headspace gas sample was stored at –20˚C for the onshore analysis of compositions of hydrocarbon gases and carbon and hydrogen isotopic compositions of methane.

9.5. Microbiology

9.5.1 Surface seawater sampling

Surface seawater was sampled at the location of 0.8 mile (around 1.3 km, 32 27.0657N, 134 13.1944E) away from the coring site, by using plastic bucket. The temperature of seawater was 27.8 ℃ at the time of sampling. Sampled surface seawater was placed in pre-sterilized plastic container (SEKISUI). The microbes in the seawater were captured onto 0.22 μm-pore sterivex filter (Millipore). After immersing the filter in RNAlater (Thermo) for overnight, the filter was stored at -80℃.

9.5.2 Hole B

The data of X-ray CT scanning were examined to find the potential horizon of volcanic ash (Tephra) layers. The identified three regions in the cores C9037B-3H-7, 10H-3 were sectioned into five pieces, and 5H-6 into 7 pieces as shown in the scheme in the Fig. 13(a). Each piece was subsampled by 20 cc and 2.5 cc syringes (3 x 20 cc, and 1 x 2.5 cc). One 20 cc syringe sample was fixed by formalin, two other 20 cc syringes were frozen, and 1 of 2.5 cc syringe sample was used for cultivation experiment. For freezing, we used CAS (cell alive system) freezer with a setting of power 80%. After syringe sampling, remaining portions of the whole round core were all stuck into one piece and returned to core flow.

For cultivation experiment, we suspended 1 cc of subsampled core in 10 mL of sterilized artificial seawater and sonicated for 1 minute using an ultrasonic homogenizer (Model UH-50, SMT Co. Ltd., Tokyo, Japan) to detach microbial cells from sediment particles. Then 100 µl of the slurry was spread on Zobel 2216E agar plate (ZoBell, 1941). Part of the plates were exposed to UV light to screen the UV-resistant microbes. The plates were stored at 4 ºC and will be incubated at 10 ºC at onshore laboratory.

9.5.3 Hole C

At hole C, we collected samples for (a) core quality study and (b) core metagenome study. At Core Cutting Area, whole round core (WRC) samples were cut, and one 20 cc syringe and one 2.5 cc syringe samples were taken from WRC for core quality study. All of the sampled WRCs were immediately transferred to Core Processing Deck and subjected to X-ray CT scanning (fast track). After X-ray CT scan, WRCs for core metagenome study were immediately transferred to CAS freezer for freezing. Another subsamples (1 of 20 cc, 1 of 2.5 cc syringes) were taken from core quality WRC after all the sections of the core were run through MSCL-W. Further subsampling is planned for the timing of core will be cut into halves at Kochi Core Center. The samples of core quality study will be examined timewise shift of microbial community structure upon analysis and storage. The metagenome samples will be used to find depth-wise shift of microbial functional genes.

At three intervals (4H, 11H, and 13H) each two 5 cm WRCs were sampled for checking ORP (oxidation/reduction potential) in the cores. One WRC was placed at cooled (~8 ºC) condition and the other WRC was placed at room temperature. ORP in the WRCs was measured by inserting microelectrode and the changes over time were recorded.

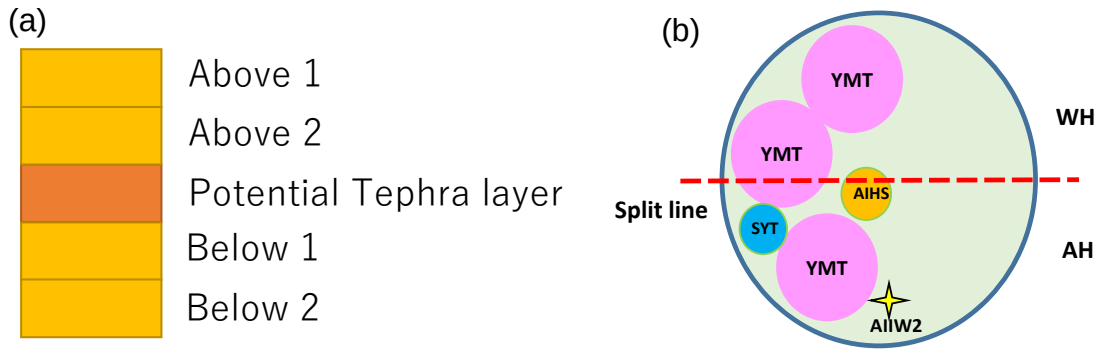

Figure 13. Sampling scheme.

10. Post-cruise study plan

10.1. Non-destructive measurements

After the expedition, the drilled cores are transported to the Kochi Core Center (KCC). KCC staff cut the drilled core in half, and describe the lithology and imaging by core scanner. Then we will conduct routine non-destructive measurements using the facilities such as spectrophotometer and XRF-core scanner ITRAX. A composite section will be established based on the results of physical properties and color reflectance.

10.2. Chronology

Chronologies will be obtained by common dating methods, radiocarbon dating of planktic foraminifers, $\delta^{18}O$ measurements on benthic foraminifera, and conventional tephrostratigraphy.

10.3. Proxy analysis for past Kuroshio variability

The KC variation will be investigated using several proxies, such as sea surface temperature (SST) from microfossil-based transfer functions, UK37, and Mg/Ca in planktic foraminifer. Vertical thermal structure in the KC will be revealed by $\delta^{18}O$ and Mg/Ca records in multi-species of planktic foraminifers with different depth habitat (Sagawa et al., 2011). Carbon isotopes of deep dweller planktic foraminifer and benthic foraminifers are used to reconstruct change of intermediate and deep water circulations. Carbon isotope in organic matters will be

used for biological productivity (Ikehara et al., 2009).

10.4. Origin and mechanisms of deep-sea turbidites

Detailed analysis of the sedimentary structure and compositions of turbidite layers is expected to provide new insights into the frequency of large-scale flood event on land and the effects of the Nankai Trough mega-earthquake, which are considered to be the mechanisms of turbidite deposition in the continental slope off Shikoku.

11. References

Ambe, D., Imawaki, S., Uchida, H., Ichikawa, K., 2004. Estimating the Kuroshio Axis South of Japan Using Combination of Satellite Altimetry and Drifting Buoys. *Journal of Oceanography*, **60**, 375-382.

Anthonissen and Ogg, 2012. Appendix 3: Cenozoic and Cretaceous biochronology of planktonic foraminifera and calcareous nannofossils. In: Gradstein, F. M., Ogg, J. G., Schmitz, M. D. and Ogg, G. M., Eds., The Geologic Time Scale 2012, 2: 1083–1127. Amsterdam, Elsevier.

Backman, J., Raffi, I., Rio, D., Fornaciari, E., Pälike, H. 2012. Biozonation and biochronology of Miocene through Pleistocene calcareous nannofossils from low and middle latitudes, *Newsletters on Stratigraphy*, **45**, 221-244, https://doi.org/10.1127/0078-0421/2012/0022.

Berger, A. and Loutre, M.F., 2002. An exceptionally long interglacial ahead?, *Science*, **297**, 1287-1288.

Bown, P.R. and Young, J.R., 1998. Techniques. In, Bown, P. R. (ed.) Calcareous Nannofossil Biostratigraphy. Chapman and Hall (Kluwer Academic Publishers), Dordrecht (1998), pp. 16-28.

Candy, I., Schreve, D.C., Sherriff, J., Tye, G.J., 2014. Marine Isotope Stage 11: Palaeoclimates, palaeoenvironments and its role as an analogue for the current interglacial. *Earth-Science Reviews*, **128**, 18-51.

Chiyonobu, S., Yamamoto, Y., Saito, S., 2017. Calcareous nannofossil biostratigraphy and geochronology of Neogene trench-slope cover sediments in the south Boso Peninsula, central Japan: Implications for the development of a shallow accretionary complex. *Tectonophysics* **710-711**, 56-68.

Domitsu, H., Uchida, J., Ogane, K., Dobuchi, N., Sato, T., Ikehara, M., Nishi, H., Hasegawa, S., Oda, M., 2011. Stratigraphic relationships between the last occurrence of *Neogloboquadrina inglei* and marine isotope stages in the northwest Pacific, D/V Chikyu Expedition 902, Hole C9001C. *Newsletters on Stratigraphy*, **44**, 113-122.

Domitsu, H. and Oda, M., 2008. Pleistocene planktic foraminiferal events in the Northwest Pacific

near Japan, *The Open Paleontology Journal*, **1**, 1-6.

Droxler, A.W., Farrell, J.W., 2000. Marine Isotope Stage 11 (MIS 11): new insights for a warm future. *Global and Planetary Change*, **24**, 1-5.

Etourneau, J., Schneider, R., Blanz, T., Martinez, P., 2010. Intensification of the Walker and Hadley atmospheric circulations during the Pliocene–Pleistocene climate transition. *Earth and Planetary Science Letters*, **297**, 103-110.

Hayashi, H., Asano, S., Yamashita, Y., Tanaka, T., and Nishi, H., 2011. Data report: late Neogene planktonic foraminiferal biostratigraphy of the Nankai Trough, IODP Expedition 315. In Kinoshita, M., Tobin, H., Ashi, J., Kimura, G., Lallemant, S., Screaton, E.J., Curewitz, D., Masago, H., Moe, K.T., and the Expedition 314/315/316 Scientists, Proc. IODP, 314/315/316: Washington, DC (Integrated Ocean Drilling Program Management International, Inc.). doi:10.2204/iodp.proc.314315316.206.2011.

Herbert, T.D., Peterson, L.C., Lawrence, K.T., Liu, Z., 2010. Tropical Ocean Temperatures Over the Past 3.5 Million Years. *Science*, **328**, 1530-1534.

Hu, D., Wu, L., Cai, W., Gupta, A.S., Ganachaud, A., Qiu, B., Gordon, A.L., Lin, X., Chen, Z., Hu, S., Wang, G., Wang, Q., Sprintall, J., Qu, T., Kashino, Y., Wang, F., Kessler, W.S., 2015. Pacific western boundary currents and their roles in climate. *Nature*, **522**, 299-308.

Ikehara, M., M. Murayama, O. Tadai, N. Hokanishi, N. Daido, H. Kawahata, and H. Yasuda, 2006. Late Quaternary tephrostratigraphy of two IMAGES cores taken from the off Shikoku in the Northwest Pacific. *Fossils*, **79**, 60-76. (in Japanese with English abstract).

Ikehara, M., Akita, D., Matsuda, A., 2009. Enhanced marine productivity in the Kuroshio region off Shikoku during the last glacial period inferred from the accumulation and carbon isotopes of sedimentary organic matter. *Journal of Quaternary Science*, **24**, 848–855.

JAMSTEC, 2004. Crustal structural database site, JAMSTEC. Doi:10.17596/0002069 (accepted 2020-05-08).

Jia, G., Chen, F., Peng, P.a., 2008. Sea surface temperature differences between the western equatorial Pacific and northern South China Sea since the Pliocene and their paleoclimatic implications. *Geophysical Research Letters*, **35**, doi:10.1029/2008GL034792.

Kawabe, M., 1995. Variations of current path, velocity, and volume transport of the Kuroshio in relation with the large meander, *Journal of Physical Oceanography*, **25**, 3103-3117.

Kimoto, K., Takaoka, H., Oda, M., Ikehara, M., Matsuoka, H., Okada, M., Oba, T., Taira, A., 2003. Carbonate dissolution and planktonic foraminiferal assemblages observed in three piston cores collected above the lysocline in the western equatorial Pacific. *Marine Micropaleontology*, **47**, 227-251.

Kucera, M. and Kennett, J.P., 2000. Biochronology and evolutionary implications of Late Neogene California margin planktonic foraminiferal events, *Marine Micropaleontology*, **40**,

67-81.

Kuwano, D., Kubota, Y., Mantoku, K., Kameo, K., 2021. Oxygen isotope stratigraphy and calcareous nannofossil biostratigraphy of the Lower Pleistocene in the Boso Peninsula, central Japan, *Stratigraphy*, **18**, 103–121.

Lea, D.W., Pak, D.K., Spero, H.J., 2000. Climate impact of Late Quaternary equatorial Pacific sea surface temperature variations. *Science*, **289**, doi:10.1126/science.289.5485.1719.

Lisiecki, L.E., Raymo, M.E., 2005. A Pliocene-Pleistocene stack of 57 globally distributed benthic records. *Paleoceanography*, **20**, doi:10.1029/2004PA001071.

Locarnini, R.A., A.V. Mishonov, J.I. Antonov, T.P. Boyer, H.E. Garcia, O.K. Baranova, M.M. Zweng, C.R. Paver, J.R. Reagan, D.R. Johnson, M. Hamilton, D. Seidov, 2013. World Ocean Atlas 2013, Volume 1: Temperature. S. Levitus, Ed.; A. Mishonov, Technical Ed.; NOAA Atlas NESDIS 73, 40pp.

Luthi, D., Le Floch, M., Bereiter, B., Blunier, T., Barnola, J.-M., Siegenthaler, U., Raynaud, D., Jouzel, J., Fischer, H., Kawamura, K., Stocker, T.F., 2008. High-resolution carbon dioxide concentration record 650,000-800,000 years before present. *Nature*, **453**, 379-382.

Machida, H., Arai, F., 2003. Atlas of tephra in and around Japan. 336p, University of Tokyo Press.

Masson-Delmotte, V., M. Schulz, A. Abe-Ouchi, J. Beer, A. Ganopolski, J.F. González Rouco, E. Jansen, K. Lambeck, J. Luterbacher, T. Naish, T. Osborn, B. Otto-Bliesner, T. Quinn, R. Ramesh, M. Rojas, X. Shao and A. Timmermann, 2013. Information from Paleoclimate Archives. In: Climate Change 2013: The Physical Science Basis. Contribution of Working Group I to the Fifth Assessment Report of the Intergovernmental Panel on Climate Change [Stocker, T.F., D. Qin, G.-K. Plattner, M. Tignor, S.K. Allen, J. Boschung, A. Nauels, Y. Xia, V. Bex and P.M. Midgley (eds.)]. Cambridge University Press, Cambridge, United Kingdom and New York, NY, USA.

Matsuzaki, M. K., Nishi, H., Hayashi, H., Suzuki, N., Gyawali, B. R., Ikehara, M., Tanaka, T., Takashima, R., 2014. Radiolarian biostratigraphic scheme and stable oxygen isotope stratigraphy in southern Japan (IODP Expedition 315 Site C0001), *Newsletters on Stratigraphy*, **47/1**, 107–130.

Matsuzaki, K.M., Suzuki, N., Nishi, H., Hayashi, H., Gyawali, B.R., Takashima, R., Ikehara, M., 2015. Early to Middle Pleistocene paleoceanographic history of southern Japan based on radiolarian data from IODP Exp. 314/315 Sites C0001 and C0002, *Marine Micropaleontology*, **118**, 17–33.

Medina-Elizalde, M., Lea, D.W., Fantle, M.S., 2008. Implications of seawater Mg/Ca variability for Plio-Pleistocene tropical climate reconstruction. *Earth and Planetary Science Letters*, **269**, 585-595.

Melles, M., Brigham-Grette, J., Minyuk, P.S., Nowaczyk, N.R., Wennrich, V., DeConto, R.M.,

Anderson, P.M., Andreev, A.A., Coletti, A., Cook, T.L., Haltia-Hovi, E., Kukkonen, M., Lozhkin, A.V., Rosén, P., Tarasov, P., Vogel, H., Wagner, B., 2012. 2.8 Million Years of Arctic Climate Change from Lake El'gygytgyn, NE Russia. *Science*, **337**, 315-320.

Moore, G.F., Taira, A., Klaus, A., et al., 2001. Proceeding of the ODP, Initial Reports, 190: College Station, TX (Ocean Drilling Program). doi:10.2973/odp.proc.ir.190.2001.

NEEM community members, 2013. Eemian interglacial reconstructed from a Greenland folded ice core. *Nature*, **493**, 489-494.

Otto-Bliesner, B.L., Rosenbloom, N., Stone, E.J., McKay, N.P., Lunt, D.J., Brady, E.C., Overpeck, J.T., 2013. How warm was the last interglacial? New model–data comparisons. *Philosophical Transactions of the Royal Society A: Mathematical, Physical and Engineering Sciences*, **371**, 10.1098/rsta.2013.0097.

Sagawa, T., Yokoyama, Y., Ikehara, M., Kuwae, M., 2011. Vertical thermal structure history in the western subtropical North Pacific since the Last Glacial Maximum, *Geophysical Research Letters*, **38**, doi:10.1029/2010GL045827.

Saito, T., Thompson, P.R., Breger, D. 1981. Systematic index of recent and Pleistocene planktonic foraminifera, University of Tokyo Press.

Sakamoto, T.T., Hasumi, H., Ishii, M., Emori, S., Suzuki, T., Nishimura, T., Sumi, A., 2005. Responses of the Kuroshio and the Kuroshio Extension to global warming in a high-resolution climate model. *Geophysical Research Letters*, **32**, doi:10.1029/2005GL023384.

Schiebel, R. and Hemleben, C. 2017. Planktic foraminifers in the modern ocean, Springer-Verlag, Berlin.

Tzedakis, P.C., 2010. The MIS 11 - MIS 1 analogy, southern European vegetation, atmospheric methane and the "early anthropogenic hypothesis". *Climate of the Past*, **6**, 131-144.

Tokuyama, H., Honza, E., Kimura, M., Kuramoto, S., Ashi, J., Okamura, N., Arato, H., Ito, Y., Soh, W., Hino, R., Nohara, T., Abe, H., Sakai, S., Mukaiyama, K., 2001. Development history of geological structure around Japanese islands after the latest Miocene, *Journal of Japan Society for Marine Surveys and Technology*, **13**, 27-53.

Turney, C.S.M., Jones, R.T., 2010. Does the Agulhas Current amplify global temperatures during super-interglacials? *Journal of Quaternary Science*, **25**, 839-843.

Uemura, R., Motoyama, H., Masson-Delmotte, V., Jouzel, J., Kawamura, K., Goto-Azuma, K., Fujita, S., Kuramoto, T., Hirabayashi, M., Miyake, T., Ohno, H., Fujita, K., Abe-Ouchi, A., Iizuka, Y., Horikawa, S., Igarashi, M., Suzuki, K., Suzuki, T., Fujii, Y., 2018. Asynchrony between Antarctic temperature and CO_2 associated with obliquity over the past 720,000 years. *Nature Communications*, **9**, 961, doi:10.1038/s41467-018-03328-3.

Wang, L., 1994. Sea surface temperature history of the low latitude western Pacific during the last 5.3 million years. *Palaeogeography, Palaeoclimatology, Palaeoecology*, **108**, 379-436.

Wu, G., Berger, W.H., 1991. Pleistocene $\delta^{18}O$ records from Ontong Java Plateau: Effects of winnowing and dissolution. *Marine Geology*, **96,** 193-209.

Wu, L., Cai, W., Zhang, L., Nakamura, H., Timmermann, A., Joyce, T., McPhaden, M.J., Alexander, M., Qiu, B., Visbeck, M., Chang, P., Giese, B., 2012. Enhanced warming over the global subtropical western boundary currents. *Nature Climate Change*, **2**, 161-166.

Yang, H., Lohmann, G., Krebs-Kanzow, U., Ionita, M., Shi, X., Sidorenko, D., Gong, X., Chen, X., Gowan, E.J., 2020. Poleward shift of the major ocean gyres detected in a warming climate. *Geophysical Research Letters*, **47**, e2019GL085868.

Young, J.R. 1998. Neogene, P.R. Bown (Ed.), Calcareous Nannofossil Biostratigraphy, Kluwer Academic Publishing, Dorderecht (1998), pp. 225-265.

Young, J.R., Bown, P.R., Lees, J.A., 2017. Nannotax3 website, International Nannoplankton Association. Accessed 21 Apr 2017. http://www.mikrotax.org/Nannotax3.

ZoBell, C.E. 1941. Studies on marine bacteria. I. The cultural requirements of heterotrophic aerobes, *Journal of Marine Research*, **4**, 41-75.

Zweng, M.M, J.R. Reagan, J.I. Antonov, R.A. Locarnini, A.V. Mishonov, T.P. Boyer, H.E. Garcia, O.K. Baranova, D.R. Johnson, D.Seidov, M.M. Biddle, 2013. World Ocean Atlas 2013, Volume 2: Salinity. S. Levitus, Ed., A. Mishonov Technical Ed.; NOAA Atlas NESDIS 74, 39.

12. Appendix

Appendix 1. Preliminary results of radiolarian assemblages of C9037.

Appendix 2. Preliminary results of nannofossil assemblages of C9037.

Appendix 3. Preliminary results of foraminifer assemblages of C9037.